

An asymptotic preserving scheme satisfying entropy stability for the barotropic Euler system*

Megala Anandan[†], Mária Lukáčová-Medvid'ová[‡], S. V. Raghurama Rao[§]

Abstract

In this paper we study structure-preserving numerical methods for low Mach number barotropic Euler equations. Besides their asymptotic preserving properties that are crucial in order to obtain uniformly consistent and stable approximations of the Euler equations in their singular limit as the Mach number approaches zero, our aim is also to preserve discrete entropy stability. Suitable acoustic/advection splitting approach combined with time implicit-explicit approximations are used to achieve the asymptotic preserving property. The entropy stability of different space discretisation strategies is studied for different values of Mach number and is validated by the numerical experiments.

1 Introduction

Many problems arising in science and engineering often contain dimensionless parameters that appear when suitable non-dimensionalisation is employed. For barotropic/full Euler systems, the Mach number appears as a parameter (denoted by ϵ), which dictates whether the flow is compressible ($\epsilon \sim \mathcal{O}(1)$) or incompressible ($\epsilon \ll 1$). The appearance of such a small parameter in the denominator also leads to stiffness in the system, reflected in wide disparity of propagating wave speeds. It has been rigorously proved in [25, 26, 35] that the solutions of such hyperbolic systems converge to those of mixed hyperbolic-elliptic incompressible system when ϵ approaches zero. Explicit numerical methods for these systems require restrictive ϵ -dependent stability condition on time step, and hence they become computationally very expensive when ϵ becomes small. Further, Godunov-type compressible flow solvers suffer from loss of accuracy as numerical dissipation is inversely proportional to ϵ [14]. Fully implicit numerical methods, on the other hand, are complicated to implement due to non-linearity of the Euler systems. Hence, attempts were made to efficiently extend the compressible flow solvers to incompressible/low Mach number limit consisting of divergence-free constraint on velocity field. In particular, semi-implicit time stepping techniques allow for the compressible solver to transform into an incompressible solver as ϵ becomes small, and its stability requirements are independent of ϵ . Such schemes are called asymptotic preserving (AP) schemes, first introduced by Jin [23] for kinetic equations and later extended to hyperbolic systems (see [24] for review). Semi-implicit time stepping is often achieved by implicit-explicit (IMEX) approach involving implicit treatment of stiff terms and explicit treatment of non-stiff terms. Several IMEX-AP schemes have been formulated by using different strategies to split the flux into stiff and non-stiff parts, and we refer the interested reader to [13, 39, 11, 21, 4, 27, 5, 15, 7, 16, 42, 6, 43, 2, 34]. In addition to asymptotic preserving properties, another crucially required property for a numerical method is its stability. For the Euler equations, this also means non-linear stability dictated by the second law of thermodynamics, the entropy inequality. Consequently, entropy stability has emerged as a non-linear stability criterion for numerical schemes since the seminal work of Tadmor [36, 37, 38]. Several entropy stable numerical methods for different hyperbolic systems have been developed. These include developments specific to shallow water equations [18, 40, 28, 1], the Euler equations [3, 22, 29, 30, 8, 31, 32, 19, 12, 10, 41], and magnetohydrodynamics equations [9]. However, these entropy stable schemes were proposed for fixed Mach number (ϵ being order one). On the other hand, the governing system is associated with an entropy inequality for all non-zero values of ϵ . Hence, our aim in this paper is to develop a numerical scheme that is entropy stable for different values of ϵ , and also AP as ϵ approaches zero. As far as we are aware, this question has not yet been studied in literature. The present paper makes the first step in this research direction, discusses possible discretisation strategies, and validates them by a series of numerical experiments.

***Funding:** Megala Anandan was funded by the Ministry of Education, Government of India under the Prime Minister's Research Fellowship/grant PM/MHRD-19-17567.03.

[†]Institute for Mathematics, Johannes Gutenberg University of Mainz, 55128 Mainz, Germany. e-mail: manandan@uni-mainz.de

[‡]Institute for Mathematics, Johannes Gutenberg University of Mainz, 55128 Mainz, Germany. e-mail: lukacova@uni-mainz.de

[§]Indian Institute of Science, Bangalore-560012, India. e-mail: raghu@iisc.ac.in

The paper is organised as follows: Section 2 presents the barotropic Euler system, its entropy stability property for different values of Mach number ϵ , and its asymptotic limit as ϵ approaches zero. Section 3 presents the numerical method that employs an IMEX-AP time discretisation in the spirit of [15, 6], and three different space discretisation strategies. The asymptotic preserving property of fully discrete scheme is also presented. Section 4 presents the numerical validation of our scheme by depicting the AP and entropy stability properties. Section 5 concludes the paper.

2 Mathematical model

In this section, we present the barotropic Euler system, its entropy stability property, and its asymptotic limit as Mach number approaches 0.

2.1 The barotropic Euler system

Consider the barotropic Euler system,

$$\partial_t \rho + \nabla \cdot (\rho \mathbf{u}) = 0 \quad (1)$$

$$\partial_t (\rho \mathbf{u}) + \nabla \cdot (\rho \mathbf{u} \otimes \mathbf{u}) + \nabla p(\rho) = \mathbf{0}, \quad (2)$$

where $\mathbf{x} \in \Omega \subset \mathbb{R}^d$, $t \in \mathbb{R}^+ \cup \{0\}$, $\rho(\mathbf{x}, t) : \Omega \times \mathbb{R}^+ \cup \{0\} \rightarrow \mathbb{R}^+$ is the fluid density, $\mathbf{u}(\mathbf{x}, t) : \Omega \times \mathbb{R}^+ \cup \{0\} \rightarrow \mathbb{R}^d$ is the fluid velocity, and $p(\rho(\mathbf{x}, t)) = \kappa \rho^\gamma \in \mathbb{R}^+$ is the pressure. Here, d is the dimension in space, and κ , $\gamma > 1$ are constants. This system is hyperbolic with eigenvalues (in direction \mathbf{n}) $\mathbf{u} \cdot \mathbf{n} - c$ and $\mathbf{u} \cdot \mathbf{n} + c$, where $c = \sqrt{\gamma p / \rho}$ is the sound speed, and the conserved quantities are density, ρ and momentum, $\rho \mathbf{u}$. The initial conditions required for the system are $\rho(\mathbf{x}, 0) = \rho^0(\mathbf{x})$ and $\mathbf{u}(\mathbf{x}, 0) = \mathbf{u}^0(\mathbf{x})$, and the boundary is considered to have periodic or zero flux conditions.

We perform non-dimensionalization of the above barotropic Euler system in (1) and (2) by using the reference values $x_r, t_r, \rho_r, u_r, p_r$. The dimensionless variables are given as,

$$\hat{\mathbf{x}} = \frac{\mathbf{x}}{x_r}, \hat{t} = \frac{t}{t_r}, \hat{\rho} = \frac{\rho}{\rho_r}, \hat{\mathbf{u}} = \frac{\mathbf{u}}{u_r}, \hat{p} = \frac{p}{p_r}. \quad (3)$$

Inserting these into (1) and (2) and omitting the hat symbol, we obtain the dimensionless barotropic Euler system,

$$\partial_t \rho + \nabla \cdot (\rho \mathbf{u}) = 0 \quad (4)$$

$$\partial_t (\rho \mathbf{u}) + \nabla \cdot (\rho \mathbf{u} \otimes \mathbf{u}) + \frac{1}{\epsilon^2} \nabla p(\rho) = \mathbf{0}, \quad (5)$$

where $\epsilon = u_r \sqrt{\rho_r / p_r}$ is proportional to the Mach number. This system is also hyperbolic, and its eigenvalues (in direction \mathbf{n}) are $\mathbf{u} \cdot \mathbf{n} - c/\epsilon$ and $\mathbf{u} \cdot \mathbf{n} + c/\epsilon$. Hereafter, we consider the dimensionless form of barotropic Euler system in (4) and (5) for the presentation of analysis and numerical methods.

2.2 Entropy stability property

Most hyperbolic systems in general have entropy inequality associated with them. In this section, we present the entropy inequality corresponding to the system in (4) and (5). As we will see in what follows, the physical energy plays the role of (mathematical) entropy. Consequently, the entropy inequality reduces to the energy dissipation property.

Let $\mathbf{U} = [\rho, \rho u_1, \dots, \rho u_d]^T$ be the vector of conserved variables and its flux vector in k^{th} direction be denoted by $\mathbf{G}^k(\mathbf{U}) = [\rho u_k, p \delta_{k1} / \epsilon^2 + \rho u_1 u_k, \dots, p \delta_{kd} / \epsilon^2 + \rho u_d u_k]^T$. Here u_i is the i^{th} component of fluid velocity \mathbf{u} . In this notation, the barotropic Euler system in (4) and (5) can be recast as:

$$\partial_t \mathbf{U} + \partial_{x_k} \mathbf{G}^k(\mathbf{U}) = \mathbf{0}. \quad (6)$$

The convex function,

$$\eta(\mathbf{U}) = \frac{1}{2} \rho \|\mathbf{u}\|_2^2 + \frac{1}{\epsilon^2} \frac{p(\rho)}{\gamma - 1} \quad (7)$$

is an entropy for the system (6) as it satisfies,

$$\eta''(\mathbf{U}) \cdot (\mathbf{G}^k)'(\mathbf{U}) \text{ is symmetric} \iff (\omega_k)'(\mathbf{U}) = \eta'(\mathbf{U}) \cdot (\mathbf{G}^k)'(\mathbf{U}). \quad (8)$$

Here ω_k is the k^{th} component of the entropy flux function $\boldsymbol{\omega}(\mathbf{U}) = \mathbf{u}(\eta(\mathbf{U}) + p(\rho)/\epsilon^2)$ corresponding to $\eta(\mathbf{U})$. For sufficiently smooth solutions, the inner product of (6) with $\eta'(\mathbf{U})$ gives entropy equality

$$\partial_t \eta(\mathbf{U}) + \partial_{x_k} \omega_k(\mathbf{U}) = 0. \quad (9)$$

For weak (non-smooth) solutions, we only get

$$\partial_t \eta(\mathbf{U}) + \partial_{x_k} \omega_k(\mathbf{U}) \leq 0 \quad (10)$$

due to the convexity of $\eta(\mathbf{U})$. Note that (10) is understood in the distributional sense.

2.3 Asymptotic limit

Our aim in this section is to define a limiting system of (4), (5) as $\epsilon \rightarrow 0$. We point out that all calculations presented below are formal assuming enough regularity of the corresponding solutions. We assume that solutions can be expanded with respect to ϵ -powers as follows:

$$\rho = \rho_0 + \epsilon \rho_1 + \epsilon^2 \rho_2 + \dots, \quad (11)$$

$$\mathbf{u} = \mathbf{u}_0 + \epsilon \mathbf{u}_1 + \epsilon^2 \mathbf{u}_2 + \dots, \quad (12)$$

$$p = p_0 + \epsilon p_1 + \epsilon^2 p_2 + \dots \quad (13)$$

The asymptotic behavior as $\epsilon \rightarrow 0$ is determined by inserting (11), (12) and (13) into the system in (4) and (5). Balancing $\mathcal{O}(\epsilon^{-2})$ terms in the momentum conservation equation, we obtain,

$$\nabla p_0 = 0.$$

Hence, p_0 is spatially constant and is function of time alone. Since $p_0 = \kappa \rho_0^\gamma$, ρ_0 is also spatially constant and is function of time alone. Similarly balancing $\mathcal{O}(\epsilon^{-1})$ terms in the momentum conservation equation, we infer that p_1 and ρ_1 are also spatial constants and are functions of only time. Now, balancing $\mathcal{O}(1)$ terms in both mass and momentum conservation equations, we get,

$$\partial_t \rho_0 + \rho_0 \nabla \cdot \mathbf{u}_0 = 0, \quad (14)$$

$$\partial_t (\rho_0 \mathbf{u}_0) + \rho_0 \nabla \cdot (\mathbf{u}_0 \otimes \mathbf{u}_0) + \nabla p_2 = \mathbf{0}. \quad (15)$$

Here p_2 is interpreted as the hydrostatic pressure. Integrating the $\mathcal{O}(1)$ mass balance in (14) on Ω , we get,

$$|\Omega| \partial_t \rho_0 = -\rho_0 \int_{\Omega} \nabla \cdot \mathbf{u}_0 d\Omega = -\rho_0 \int_{\partial\Omega} \mathbf{u}_0 \cdot \mathbf{n} ds. \quad (16)$$

Taking $\mathbf{u} \cdot \mathbf{n} = 0$ on $\partial\Omega$ or considering periodic boundary conditions, we get $\int_{\partial\Omega} \mathbf{u}_0 \cdot \mathbf{n} ds = 0$. Thus, $\partial_t \rho_0 = 0$ and ρ_0 is constant in both space and time, resulting in $\nabla \cdot \mathbf{u}_0 = 0$ according to (14). The $\mathcal{O}(1)$ momentum balance in (15) therefore becomes,

$$\partial_t \mathbf{u}_0 + \nabla \cdot (\mathbf{u}_0 \otimes \mathbf{u}_0) + \frac{\nabla p_2}{\rho_0} = \mathbf{0}. \quad (17)$$

Similarly, integration of $\mathcal{O}(\epsilon)$ mass balance equation and usage of $\mathbf{u} \cdot \mathbf{n} = 0$ on $\partial\Omega$ or periodic boundary conditions result in $\partial_t \rho_1 = 0$, and hence ρ_1 is constant in both space and time.

Further, the initial conditions are assumed to be compatible with the equations of different orders of ϵ (such as, ϵ^{-2} , ϵ^{-1} , ϵ^0). In this paper, we consider the well-prepared initial conditions,

$$\rho(\mathbf{x}, 0) = \rho^0(\mathbf{x}) = \rho_0^0 + \epsilon^2 \rho_2^0(\mathbf{x}) \quad (18)$$

$$u(\mathbf{x}, 0) = u^0(\mathbf{x}) = u_0^0(\mathbf{x}) + \epsilon u_1^0(\mathbf{x}) \quad (19)$$

such that ρ_0^0 is constant and $\nabla \cdot \mathbf{u}_0^0 = 0$.

3 Numerical method

In this section, we want to construct a numerical method that is both asymptotic preserving and entropy stable. That is, we expect the method to satisfy the asymptotic limits of dimensionless barotropic Euler system in (4) and (5) as $\epsilon \rightarrow 0$, and also satisfy discrete entropy inequality in different regimes of ϵ . To achieve this goal, we use implicit-explicit (IMEX) time discretisation required for attaining asymptotic consistency, and compare the entropy stability property of three different types of space discretisation in different regimes of ϵ . We also present the asymptotic preserving property of considered numerical methods.

3.1 Semi-discrete IMEX time discretisation

We begin with the presentation of first order IMEX time discretisation of the barotropic Euler system in (4) and (5) for clarity.

$$\rho^{n+1} = \rho^n - \Delta t_n \nabla \cdot (\rho \mathbf{u})^{n+1} \quad (20)$$

$$(\rho \mathbf{u})^{n+1} = (\rho \mathbf{u})^n - \Delta t_n \nabla \cdot (\rho \mathbf{u} \otimes \mathbf{u})^n - \frac{\Delta t_n}{\epsilon^2} \nabla p(\rho)^{n+1} \quad (21)$$

Here, $\Delta t_n = t_{n+1} - t_n$. The mass flux $\nabla \cdot (\rho \mathbf{u})$ and the pressure term $\frac{1}{\epsilon^2} \nabla p(\rho)$ are treated implicitly, while $\nabla \cdot (\rho \mathbf{u} \otimes \mathbf{u})$ in the momentum flux is treated explicitly. It is important to treat the mass flux implicitly in order to get $\nabla \cdot \mathbf{u}^{n+1} = 0$ as $\mathcal{O}(1)$ constraint. Indeed, if the mass flux is treated explicitly, then the whole method would become explicit and require severe ϵ dependent time step restriction enforced by stability. Substituting the momentum equation (21) in $\nabla \cdot (\rho \mathbf{u})^{n+1}$ of (20), we get,

$$\rho^{n+1} = \rho^n - \Delta t_n \nabla \cdot (\rho \mathbf{u})^n + \Delta t_n^2 \nabla^2 : (\rho \mathbf{u} \otimes \mathbf{u})^n + \frac{\Delta t_n^2}{\epsilon^2} \Delta p(\rho)^{n+1}. \quad (22)$$

Since $p(\rho) = \kappa \rho^\gamma$, the presence of $\Delta p(\rho)^{n+1}$ in the above equation calls for a need to use the non-linear iterative solver to find ρ^{n+1} . To avoid the computational effort, we perform linearisation of $p(\rho)^{n+1}$ around the incompressible constant density ρ_0 as:

$$p(\rho)^{n+1} = p(\rho_0) + (\rho^{n+1} - \rho_0) p'(\rho)|_{\rho=\rho_0} + \mathcal{O}(\epsilon^4). \quad (23)$$

The above linearisation is true if the higher derivatives of p are $\mathcal{O}(1)$ and the method is asymptotic preserving (that is, $(\rho^{n+1} - \rho_0) \simeq \mathcal{O}(\epsilon^2)$). We intend to construct our method such that it is asymptotic preserving, and we have used this information *a priori* in the linearisation of $p(\rho)^{n+1}$. Using this linearisation in (22), we get,

$$\rho^{n+1} = \rho^n - \Delta t_n \nabla \cdot (\rho \mathbf{u})^n + \Delta t_n^2 \nabla^2 : (\rho \mathbf{u} \otimes \mathbf{u})^n + \frac{\Delta t_n^2}{\epsilon^2} p'(\rho)|_{\rho=\rho_0} \Delta \rho^{n+1} + \mathcal{O}(\Delta t_n^2 \epsilon^2). \quad (24)$$

In a crude sense, the modified or equivalent partial differential equation of the above time discrete equation is,

$$\partial_t \rho = -\nabla \cdot (\rho \mathbf{u})^{n+1} + \mathcal{O}(\Delta t_n) + \mathcal{O}(\Delta t_n \epsilon^2).$$

Thus, the first order temporal accuracy of the method remains unaffected due to the linearisation as long as $\mathcal{O}(\epsilon^2) \leq \mathcal{O}(1)$. The higher derivatives are considered to be $\mathcal{O}(1)$ in this argument.

As indicated by (24), (21), we have split the part governed by the acoustic waves from the rest non-stiff part. The later models the nonlinear advection waves.

From the algorithmic viewpoint, (24) can be solved easily by inversion of a matrix as follows,

$$\rho^{n+1} = \left(I - \left(\frac{\Delta t_n}{\epsilon} \right)^2 p'(\rho)|_{\rho=\rho_0} \Delta \right)^{-1} \left(\rho^n - \Delta t_n \nabla \cdot (\rho \mathbf{u})^n + \Delta t_n^2 \nabla^2 : (\rho \mathbf{u} \otimes \mathbf{u})^n \right). \quad (25)$$

Then, ρ^{n+1} evaluated as above is used to find $p(\rho)^{n+1}$. Inserting this into (21), we get $(\rho \mathbf{u})^{n+1}$ and thus the algorithm is complete. (25) and (21) together form the update equations for first order time semi-discrete scheme.

Next, we present the higher order IMEX Runge Kutta (IMEX-RK) time discretisation of the barotropic Euler system in (4) and (5). An IMEX-RK time discretisation is represented by the following double Butcher tableau:

$$\begin{array}{c|c} \tilde{c} & \tilde{A} \\ \hline & \tilde{b}^T \end{array} \quad \begin{array}{c|c} c & A \\ \hline & b^T \end{array} \quad (26)$$

where $\tilde{A} = (\tilde{a}_{ij})$, $A = (a_{ij}) \in \mathbb{R}^{s \times s}$; $c, \tilde{c}, b, \tilde{b} \in \mathbb{R}^s$. The matrices \tilde{A}, A correspond to explicit (strictly lower triangular matrix with diagonal elements as 0) and implicit (lower triangular with non-zero diagonal elements) parts of the scheme. Such A are known as *diagonally implicit* matrices. The coefficients \tilde{c} and c are given by

$$\tilde{c}_i = \sum_{j=1}^{i-1} \tilde{a}_{ij}, c_i = \sum_{j=1}^i a_{ij}, \quad (27)$$

and the vectors $\tilde{b} = (\tilde{b}_j)$ and $b = (b_j)$ give quadrature weights that combine the stages. For AP schemes, it turns to be important to work with globally stiffly accurate (GSA) IMEX-RK scheme that satisfies the following property:

$$c_s = \tilde{c}_s = 1 \text{ and } a_{sj} = b_j, \tilde{a}_{sj} = \tilde{b}_j, \quad \forall j \in \{1, 2, \dots, s\}. \quad (28)$$

The GSA property ensures that the update at t_{n+1} is same as the update at s^{th} stage. The i^{th} stage update (for $i \in \{1, 2, \dots, s\}$) of the barotropic Euler system in (4) and (5) is given by,

$$\rho^i = \rho^n - \Delta t_n \sum_{j=1}^i a_{ij} \nabla \cdot (\rho \mathbf{u})^j \quad (29)$$

$$(\rho \mathbf{u})^i = (\rho \mathbf{u})^n - \Delta t_n \sum_{j=1}^{i-1} \tilde{a}_{ij} \nabla \cdot (\rho \mathbf{u} \otimes \mathbf{u})^j - \frac{\Delta t_n}{\epsilon^2} \sum_{j=1}^i a_{ij} \nabla p(\rho)^j \quad (30)$$

where $\Delta t_n = t_{n+1} - t_n$. Substituting the momentum equation (30) in $\nabla \cdot (\rho \mathbf{u})^i$ of (29), we get,

$$\rho^i = \rho^n - \Delta t_n \sum_{j=1}^{i-1} a_{ij} \nabla \cdot (\rho \mathbf{u})^j - \Delta t_n a_{ii} \nabla \cdot (\rho \mathbf{u})^n + \Delta t_n^2 a_{ii} \sum_{j=1}^{i-1} \tilde{a}_{ij} \nabla^2 : (\rho \mathbf{u} \otimes \mathbf{u})^j + \frac{\Delta t_n^2}{\epsilon^2} a_{ii} \sum_{j=1}^i a_{ij} \Delta p(\rho)^j. \quad (31)$$

The above equation requires a nonlinear solver to find ρ^i . Similar to first order method, we perform linearisation around incompressible constant density ρ_0 :

$$p(\rho)^i = p(\rho_0) + (\rho^i - \rho_0) p'(\rho)|_{\rho=\rho_0} + \mathcal{O}(\epsilon^4). \quad (32)$$

The asymptotic preserving property ($(\rho^i - \rho_0) \simeq \mathcal{O}(\epsilon^2)$) of the method is used a priori in the linearisation. Plugging in (31) yields,

$$\begin{aligned} \rho^i &= \left(I - \left(\frac{\Delta t_n}{\epsilon} \right)^2 a_{ii}^2 p'(\rho)|_{\rho=\rho_0} \Delta \right)^{-1} \\ &\left(\rho^n - \Delta t_n \sum_{j=1}^{i-1} a_{ij} \nabla \cdot (\rho \mathbf{u})^j - \Delta t_n a_{ii} \nabla \cdot (\rho \mathbf{u})^n + \Delta t_n^2 a_{ii} \sum_{j=1}^{i-1} \tilde{a}_{ij} \nabla^2 : (\rho \mathbf{u} \otimes \mathbf{u})^j + \frac{\Delta t_n^2}{\epsilon^2} a_{ii} \sum_{j=1}^{i-1} a_{ij} p'(\rho)|_{\rho=\rho_0} \Delta \rho^j \right). \end{aligned} \quad (33)$$

Then, ρ^i evaluated as above is used to find $p(\rho)^i$. Inserting this into (30), we get $(\rho \mathbf{u})^i$ and thus the evaluation of stage values is complete. (33) and (30) together form the stage update equations for higher order IMEX-RK time semi-discrete scheme. Further, $\rho^{n+1} = \rho^s$ and $(\rho \mathbf{u})^{n+1} = (\rho \mathbf{u})^s$ due to the GSA property and therefore the algorithm is complete.

3.2 Asymptotic preserving property of the time semi-discrete scheme

In this section, we show that the higher order GSA IMEX-RK time semi-discrete scheme (31) and (30) is asymptotic preserving.

Theorem 1. *Assume well-prepared initial conditions in (18) and (19), the asymptotic expansion in (11)-(13), and periodic boundary conditions on ρ and \mathbf{u} . Then the time semi-discrete GSA IMEX-RK scheme given by (31) and (30) satisfies for $\epsilon \rightarrow 0$*

$$\rho_0^i \equiv \text{constant}, \quad \rho_1^i \equiv \text{constant}, \quad \rho_0^i + \epsilon \rho_1^i = \rho_0, \quad (34)$$

$$\nabla \cdot \mathbf{u}_0^i = 0, \quad (35)$$

$$\mathbf{u}_0^i = \mathbf{u}_0^n - \Delta t_n \sum_{j=1}^{i-1} \tilde{a}_{ij} \nabla \cdot (\mathbf{u}_0 \otimes \mathbf{u}_0)^j - \frac{\Delta t_n}{\rho_0} \sum_{j=1}^i a_{ij} \nabla p_2^j, \quad (36)$$

for all $i \in \{1, 2, \dots, s\}$, which is a consistent approximation of the incompressible Euler system (14), (15).

Proof. Inserting the asymptotic expansion (11)-(13) into the momentum update equation (30) and equating $\mathcal{O}(\frac{1}{\epsilon^2})$ terms, we obtain

$$\Delta t_n \sum_{j=1}^i a_{ij} \nabla p_0^j = 0, \quad \text{for all } i \in \{1, 2, \dots, s\} \implies \nabla p_0^i = 0, \quad \text{for all } i \in \{1, 2, \dots, s\}.$$

Since $p_0^i = \kappa \rho_0^{i\gamma}$, ρ_0^i is spatially constant for all $i \in \{1, 2, \dots, s\}$. Similarly equating $\mathcal{O}(\frac{1}{\epsilon})$ terms in the momentum update equation (30), we infer that ρ_1^i is spatially constant for all $i \in \{1, 2, \dots, s\}$.

Inserting the asymptotic expansion (11)-(13) into the mass update equation (31) and equating $\mathcal{O}(1)$ terms, we obtain

$$\rho_0^i = \rho_0^n - \Delta t_n \sum_{j=1}^{i-1} a_{ij} \rho_0^j \nabla \cdot (\mathbf{u}_0)^j - \Delta t_n a_{ii} \rho_0^n \nabla \cdot (\mathbf{u}_0)^n + \Delta t_n^2 a_{ii} \sum_{j=1}^{i-1} \tilde{a}_{ij} \rho_0^j \nabla^2 : (\mathbf{u}_0 \otimes \mathbf{u}_0)^j + \Delta t_n^2 a_{ii} \sum_{j=1}^i a_{ij} \Delta p_2^j. \quad (37)$$

Integrating the above equation on Ω and using periodic boundary conditions on ρ_2 and \mathbf{u}_0 , we obtain

$$\rho_0^i = \rho_0^n, \quad \text{for all } i \in \{1, 2, \dots, s\}. \quad (38)$$

Repeating the similar procedure for $\mathcal{O}(\epsilon)$ terms of the mass update equation (31), we obtain,

$$\rho_1^i = \rho_1^n, \quad \text{for all } i \in \{1, 2, \dots, s\}. \quad (39)$$

Since $\rho_{0,1}^{n+1} = \rho_{0,1}^s$ due to the GSA property of IMEX-RK time discretisation, we have $\rho_{0,1}^{n+1} = \rho_{0,1}^s = \rho_{0,1}^n$. Therefore, $\rho_{0,1}^n = \rho_{0,1}^0 \equiv \text{constant}$, for all $n = 1, 2, \dots$.

Inserting this into the $\mathcal{O}(1)$ mass and momentum update equations, we get for all $i \in \{1, 2, \dots, s\}$

$$\sum_{j=1}^{i-1} a_{ij} \nabla \cdot (\mathbf{u}_0)^j + a_{ii} \nabla \cdot (\mathbf{u}_0)^n - \Delta t_n a_{ii} \sum_{j=1}^{i-1} \tilde{a}_{ij} \nabla^2 : (\mathbf{u}_0 \otimes \mathbf{u}_0)^j - \frac{\Delta t_n}{\rho_0} a_{ii} \sum_{j=1}^i a_{ij} \Delta p_2^j = 0, \quad (40)$$

$$\mathbf{u}_0^i = \mathbf{u}_0^n - \Delta t_n \sum_{j=1}^{i-1} \tilde{a}_{ij} \nabla \cdot (\mathbf{u}_0 \otimes \mathbf{u}_0)^j - \frac{\Delta t_n}{\rho_0} \sum_{j=1}^i a_{ij} \nabla p_2^j, \quad (41)$$

where $\rho_0 = \rho_0^0 + \epsilon \rho_1^0$. Taking divergence of (41) and inserting it into (40), we obtain

$$\sum_{j=1}^i a_{ij} \nabla \cdot (\mathbf{u}_0)^j = 0, \quad \text{for all } i \in \{1, 2, \dots, s\} \implies \nabla \cdot (\mathbf{u}_0)^i = 0, \quad \text{for all } i \in \{1, 2, \dots, s\}. \quad (42)$$

□

The above theorem shows the asymptotic consistency of the IMEX-RK time semi-discrete scheme. Due to the GSA property, the expressions for $\rho_0^s, \rho_1^s, u_0^s$ follow for $\rho_0^{n+1}, \rho_1^{n+1}, u_0^{n+1}$. In the next section, we explain the discretisation techniques for spatial derivatives present in the scheme.

3.3 Space discretisation

In this section, we discuss various consistent spatial discretisations for the time semi-discrete scheme proposed above. It is important to keep the numerical diffusion coefficients free of the small parameter ϵ , in-order to avoid an uncontrollable growth in numerical diffusion term as $\epsilon \rightarrow 0$. In what follows, we present three different types of space discretisation.

We consider the first order time semi-discrete scheme given by (25) and (21) for presentation of the spatial discretisation. The discretisation of all the spatial derivatives present in this scheme will be explained. The corresponding spatial derivatives in higher order time semi-discrete scheme given by (33) and (30) will be approximated analogously. The additional terms $\sum_{j=1}^{i-1} a_{ij} \nabla \cdot (\rho \mathbf{u})^j$ and $\sum_{j=1}^{i-1} a_{ij} \Delta p(\rho)^j$ present in the mass update equation (given by (33)) will also follow the same discretisation as $\nabla \cdot (\rho \mathbf{u})^n$ and $\Delta p(\rho)^{n+1}$ respectively. For convenience of presentation, we explain the ideas for one-dimensional setting.

3.3.1 Type 1

We apply an upwind discretisation for $\nabla \cdot (\rho \mathbf{u} \otimes \mathbf{u})^n$ in the momentum equation (21), while all other first and second derivatives present in the scheme (25) and (21) are treated in a central fashion. Since our goal is to achieve entropy stability, we do not add numerical diffusion to implicit terms as they are entropy stable with central discretisation.

1. Spatial discretisation of $\nabla \cdot (\rho \mathbf{u} \otimes \mathbf{u})^n$ in momentum equation (21) is given by upwind discretisation

$$D_{upw}(\rho \mathbf{u} \otimes \mathbf{u})_k := \frac{1}{\Delta x} \left((\rho \mathbf{u} \mathbf{u})_{k+\frac{1}{2}} - (\rho \mathbf{u} \mathbf{u})_{k-\frac{1}{2}} \right) \quad (43)$$

$$(\rho \mathbf{u} \mathbf{u})_{k+\frac{1}{2}} = \begin{cases} (\rho \mathbf{u})_k \mathbf{u}_{k+\frac{1}{2}} & \text{if } \mathbf{u}_{k+\frac{1}{2}} > 0 \\ (\rho \mathbf{u})_{k+1} \mathbf{u}_{k+\frac{1}{2}} & \text{if } \mathbf{u}_{k+\frac{1}{2}} < 0 \end{cases} \quad (44)$$

where $\mathbf{u}_{k+\frac{1}{2}} = \frac{1}{2}(\mathbf{u}_k + \mathbf{u}_{k+1})$, $k = 1, 2, \dots$ is an index of spatial discretisation.

2. Spatial discretisation of $\nabla \cdot (\rho \mathbf{u})^n$ in mass update equation (25) and $\nabla p(\rho)^{n+1}$ in momentum equation (21) are given by central finite difference discretisations

$$D_{cen}(\rho \mathbf{u})_k := \frac{1}{2\Delta x} ((\rho \mathbf{u})_{k+1} - (\rho \mathbf{u})_{k-1}) \quad (45)$$

$$D_{cen}(p)_k := \frac{1}{2\Delta x} (p_{k+1} - p_{k-1}). \quad (46)$$

3. Spatial discretisation of $\nabla^2 : (\rho \mathbf{u} \otimes \mathbf{u})^n$ and Δp^{n+1} in mass update equation (25) are given by central finite difference discretisations

$$D^2(\rho \mathbf{u} \otimes \mathbf{u})_k := \frac{1}{\Delta x^2} ((\rho \mathbf{u} \mathbf{u})_{k+1} - 2(\rho \mathbf{u} \mathbf{u})_k + (\rho \mathbf{u} \mathbf{u})_{k-1}) \quad (47)$$

$$D^2(p)_k := \frac{1}{\Delta x^2} (p_{k+1} - 2p_k + p_{k-1}), k = 1, 2, \dots \quad (48)$$

The corresponding terms in higher order time semi-discrete scheme given by (33) and (30) also follow the same discretisation as described above.

3.3.2 Type 2

All the terms in (25) and (21) follow the discretisation in type 1, except that the term $\nabla \cdot (\rho \mathbf{u})^n$ in the mass update equation (25) is treated in an upwind fashion. Spatial discretisation for $\nabla \cdot (\rho \mathbf{u})^n$ is given by,

$$D_{upw}(\rho \mathbf{u})_k := \frac{1}{\Delta x} ((\rho \mathbf{u})_{k+\frac{1}{2}} - (\rho \mathbf{u})_{k-\frac{1}{2}}) \quad (49)$$

$$(\rho \mathbf{u})_{k+\frac{1}{2}} = \begin{cases} \rho_k \mathbf{u}_{k+\frac{1}{2}} & \text{if } \mathbf{u}_{k+\frac{1}{2}} > 0 \\ \rho_{k+1} \mathbf{u}_{k+\frac{1}{2}} & \text{if } \mathbf{u}_{k+\frac{1}{2}} < 0 \end{cases} \quad (50)$$

where $\mathbf{u}_{k+\frac{1}{2}} = \frac{1}{2}(\mathbf{u}_k + \mathbf{u}_{k+1})$. The corresponding terms in higher order time semi-discrete scheme given by (33) and (30) also follow the same discretisation as described above.

3.3.3 Type 3

Here, all the terms in (25) and (21) follow the discretisation in type 1, except that the term $\nabla \cdot (\rho \mathbf{u} \otimes \mathbf{u})^n$ in momentum equation (21) is discretised by using an entropy stable flux. We apply the entropy conservative flux discretisation, and add numerical diffusion for attaining entropy stability. We first derive the entropy conserving and stable fluxes for the full barotropic Euler system, and use only the part of these fluxes corresponding to $\nabla \cdot (\rho \mathbf{u} \otimes \mathbf{u})^n$ in momentum equation (21). All other first and second derivatives in the scheme (25) and (21) are treated in central fashion as in type 1.

In one space dimension, the entropy variable corresponding to the convex entropy function (7) is:

$$\mathbf{V} = \frac{\partial \eta}{\partial \mathbf{U}} = [-\frac{1}{2}u_1^2 + \frac{1}{\epsilon^2} \frac{\kappa \gamma}{\gamma-1} \rho^{\gamma-1} \quad u_1]^T \quad (51)$$

The one-dimensional flux function is, $\mathbf{G} = [\rho u_1 \quad \frac{1}{\epsilon^2} p + \rho u_1^2]^T$. For entropy conservation, we require (cf. [36, 37, 38])

$$[\mathbf{V} \cdot \mathbf{G}]_{k+\frac{1}{2}} - [\mathbf{V}]_{k+\frac{1}{2}} \cdot \mathbf{G}_{k+\frac{1}{2}}^* = [\omega]_{k+\frac{1}{2}} \quad (52)$$

where $[\cdot]_{k+\frac{1}{2}} = (\cdot)_{k+1} - (\cdot)_k$. Thus, we get

$$[\mathbf{V} \cdot \mathbf{G}]_{k+\frac{1}{2}} - [\omega]_{k+\frac{1}{2}} = \left[\frac{1}{\epsilon^2} \frac{2\gamma-1}{\gamma-1} p(\rho) u_1 + \frac{1}{2} \rho u_1^3 \right]_{k+\frac{1}{2}} - \left[\frac{1}{2} \rho u_1^3 + \frac{1}{\epsilon^2} \frac{\gamma}{\gamma-1} p(\rho) u_1 \right]_{k+\frac{1}{2}} = \left[\frac{1}{\epsilon^2} p(\rho) u_1 \right]_{k+\frac{1}{2}}, \quad (53)$$

$$[\mathbf{V}]_{k+\frac{1}{2}} \cdot \mathbf{G}_{k+\frac{1}{2}}^* = -\frac{1}{2} [u_1^2]_{k+\frac{1}{2}} (\rho u_1)_{k+\frac{1}{2}}^* + \frac{1}{\epsilon^2} \frac{\kappa \gamma}{\gamma-1} [\rho^{\gamma-1}]_{k+\frac{1}{2}} (\rho u_1)_{k+\frac{1}{2}}^* + \frac{1}{\epsilon^2} [u_1]_{k+\frac{1}{2}} p_{k+\frac{1}{2}}^* + [u_1]_{k+\frac{1}{2}} (\rho u_1^2)_{k+\frac{1}{2}}^*. \quad (54)$$

The following interface flux function

$$\mathbf{G}_{k+\frac{1}{2}}^* = \begin{bmatrix} (\rho u_1)_{k+\frac{1}{2}}^* \\ (\frac{1}{\epsilon^2} p + \rho u_1^2)_{k+\frac{1}{2}}^* \end{bmatrix} = \begin{bmatrix} \bar{\rho}_{\gamma_{k+\frac{1}{2}}} \bar{u}_{1k+\frac{1}{2}} \\ \frac{1}{\epsilon^2} \bar{p}_{k+\frac{1}{2}} + \bar{\rho}_{\gamma_{k+\frac{1}{2}}} \bar{u}_{1k+\frac{1}{2}}^2 \end{bmatrix} \quad (55)$$

with

$$\bar{\rho}_{\gamma_{k+\frac{1}{2}}} = \frac{\gamma-1}{\gamma} \frac{[\rho^\gamma]_{k+\frac{1}{2}}}{[\rho^{\gamma-1}]_{k+\frac{1}{2}}}, \quad \bar{u}_{1_{k+\frac{1}{2}}} = \frac{1}{2} (u_{1_{k+1}} + u_{1_k}), \quad \bar{p}_{k+\frac{1}{2}} = \frac{1}{2} (p_{k+1} + p_k) \quad (56)$$

satisfies the entropy conserving condition in (52). Hence, the entropy conserving spatial discretisation of $\nabla \cdot (\rho \mathbf{u} \otimes \mathbf{u})^n$ in momentum equation (21) is given by

$$D_{EC}(\rho \mathbf{u} \otimes \mathbf{u})_k = \frac{1}{\Delta x} \left((\rho u_1^2)_{k+\frac{1}{2}}^* - (\rho u_1^2)_{k-\frac{1}{2}}^* \right) \quad (57)$$

$$(\rho u_1^2)_{k+\frac{1}{2}}^* = \bar{\rho}_{\gamma_{k+\frac{1}{2}}} \bar{u}_{1_{k+\frac{1}{2}}}^2. \quad (58)$$

Note that (57), (58) yield second order accurate approximation.

To achieve entropy stability, we consider a dissipation matrix that is independent of ϵ :

$$\Lambda = \begin{bmatrix} |\bar{u}_{1_{k+\frac{1}{2}}}| & 0 \\ 0 & |\bar{u}_{1_{k+\frac{1}{2}}}| \end{bmatrix}. \quad (59)$$

Thus, the entropy stable flux for full barotropic Euler system becomes,

$$\mathbf{G}_{k+\frac{1}{2}} = \mathbf{G}_{k+\frac{1}{2}}^* - \frac{q}{2} \Lambda [\mathbf{V}]_{k+\frac{1}{2}}, \quad (60)$$

where $q > 0$ is a suitable constant. This entropy stable flux results in first order spatial accuracy. For second order accuracy, we use (cf. [17])

$$\mathbf{G}_{k+\frac{1}{2}} = \mathbf{G}_{k+\frac{1}{2}}^* - \frac{q}{2} \Lambda \langle \langle \mathbf{V} \rangle \rangle_{k+\frac{1}{2}} \quad (61)$$

$$\langle \langle \mathbf{V} \rangle \rangle_{k+\frac{1}{2}} = [\mathbf{V}]_{k+\frac{1}{2}} - \frac{1}{2} \left(\mu \left([\mathbf{V}]_{k+\frac{1}{2}}, [\mathbf{V}]_{k+\frac{3}{2}} \right) + \mu \left([\mathbf{V}]_{k-\frac{1}{2}}, [\mathbf{V}]_{k+\frac{1}{2}} \right) \right) \quad (62)$$

$$\mu(A, B) = \begin{cases} s \min(|A|, |B|) & \text{if } s = \text{sign}(A) = \text{sign}(B) \\ 0 & \text{otherwise} \end{cases}. \quad (63)$$

Thus, the entropy stable spatial discretisation of $\nabla \cdot (\rho \mathbf{u} \otimes \mathbf{u})^n$ in momentum equation (21) is given by,

$$D_{ES}(\rho \mathbf{u} \otimes \mathbf{u})_k = \frac{1}{\Delta x} \left((\rho u_1^2)_{k+\frac{1}{2}} - (\rho u_1^2)_{k-\frac{1}{2}} \right) \quad (64)$$

$$(\rho u_1^2)_{k+\frac{1}{2}} = (\rho u_1^2)_{k+\frac{1}{2}}^* - \frac{q}{2} |\bar{u}_{1_{k+\frac{1}{2}}}| \left\{ \begin{aligned} & [u_1]_{k+\frac{1}{2}} & 1^{st} \text{ order} \\ & \langle \langle u_1 \rangle \rangle_{k+\frac{1}{2}} & 2^{nd} \text{ order} \end{aligned} \right. = \begin{cases} |\bar{u}_{1_{k+\frac{1}{2}}}| \left(\bar{\rho}_{\gamma_{k+\frac{1}{2}}} |\bar{u}_{1_{k+\frac{1}{2}}}| - \frac{q}{2} [u_1]_{k+\frac{1}{2}} \right), & 1^{st} \text{ order} \\ |\bar{u}_{1_{k+\frac{1}{2}}}| \left(\bar{\rho}_{\gamma_{k+\frac{1}{2}}} |\bar{u}_{1_{k+\frac{1}{2}}}| - \frac{q}{2} \langle \langle u_1 \rangle \rangle_{k+\frac{1}{2}} \right), & 2^{nd} \text{ order} \end{cases} \quad (65)$$

Hence, in this type, $\nabla \cdot (\rho \mathbf{u} \otimes \mathbf{u})^n$ in momentum equation (21) is discretised as shown in (64)-(65). All the other first and second derivatives present in (25) and (21) are discretised in central fashion as shown in type 1.

The corresponding terms in higher order time semi-discrete scheme given by (33) and (30) also follow the same discretisation as described above.

3.4 Asymptotic preserving property of the fully discrete scheme

In this section, we show the asymptotic consistency of our fully discrete scheme as $\epsilon \rightarrow 0$. For this, we present a general theorem that considers all the three types of spatial discretisation.

Theorem 2. Assume well-prepared initial conditions in (18) and (19), the asymptotic expansion in (11)-(13), and periodic boundary conditions on ρ and u_1 . Consider the fully discrete scheme

$$\rho_k^i = \rho_k^n - \Delta t_n \sum_{j=1}^{i-1} a_{ij} D(\rho u_1)_k^j - \Delta t_n a_{ii} D(\rho u_1)_k^n + \Delta t_n^2 a_{ii} \sum_{j=1}^{i-1} \tilde{a}_{ij} D^2(\rho u_1)_k^j + \frac{\Delta t_n^2}{\epsilon^2} a_{ii} \sum_{j=1}^i a_{ij} D^2(p)_k^j \quad (66)$$

$$(\rho u_1)_k^i = (\rho u_1)_k^n - \Delta t_n \sum_{j=1}^{i-1} \tilde{a}_{ij} D_1(\rho u_1)_k^j - \frac{\Delta t_n}{\epsilon^2} \sum_{j=1}^i a_{ij} D_{cen}(p)_k^j \quad (67)$$

with D as D_{cen} or D_{upw} , and D_1 as D_{upw} or D_{ES} . Then for $\epsilon \rightarrow 0$, a solution of (66), (67) satisfies

$$\rho_{0_k}^i \equiv \text{constant}, \quad \rho_{1_k}^i \equiv \text{constant}, \quad \rho_{0_k}^i + \epsilon \rho_{1_k}^i = \rho_0, \quad (68)$$

$$(u_{1_0})_k^i = (u_{1_0})_k^n - \Delta t_n \sum_{j=1}^{i-1} \tilde{a}_{ij} D_1(u_{1_0})_k^j - \frac{\Delta t_n}{\rho_0} \sum_{j=1}^i a_{ij} D_{cen}(p_2)_k^j, \quad (69)$$

for all $k = 1, 2, \dots$, and all $i \in \{1, 2, \dots, s\}$.

Proof. Substituting the asymptotic expansion into the momentum update equation in (67) and equating $\mathcal{O}(\frac{1}{\epsilon^2})$ terms, we get

$$\sum_{j=1}^i a_{ij} D_{cen}(p_0)_k^j = 0, \quad \text{for all } i \in \{1, 2, \dots, s\} \implies D_{cen}(p_0)_k^i = 0, \quad \text{for all } i \in \{1, 2, \dots, s\}. \quad (70)$$

Note that this property does not allow us to conclude that $(p_0)_k^i$ is spatially constant. Depending on boundary conditions, checkerboard modes could occur. In order to conclude that $(p_0)_k^i$ is spatially constant, it is required to consider a ghost point on the left and impose $p_{0_{ghost}} = (p_0)_{k=0}$. Then, $(p_0)_k^i$ is spatially constant and hence $(\rho_0)_k^i$ is also spatially constant since $(p_0)_k^i = \kappa((\rho_0)_k^i)^\gamma$.

Similarly equating $\mathcal{O}(\frac{1}{\epsilon})$ terms in the momentum balance (67), we infer that $(\rho_1)_k^i$ is spatially constant. Inserting the asymptotic expansion into the mass update equation in (66) and equating $\mathcal{O}(1)$ terms, we obtain,

$$\rho_{0_k}^i = \rho_{0_k}^n - \Delta t_n \sum_{j=1}^{i-1} a_{ij} \rho_{0_k}^j D(u_{1_0})_k^j - \Delta t_n a_{ii} \rho_{0_k}^n D(u_{1_0})_k^n + \Delta t_n^2 a_{ii} \sum_{j=1}^{i-1} \tilde{a}_{ij} \rho_{0_k}^j D^2(u_{1_0})_k^j + \Delta t_n^2 a_{ii} \sum_{j=1}^i a_{ij} D^2(p_2)_k^j. \quad (71)$$

Summing over all the points in the domain and using periodic boundary conditions on ρ_2 and u_{1_0} , we obtain,

$$\rho_{0_k}^i = \rho_{0_k}^n, \quad \text{for all } k, \quad \text{for all } i \in \{1, 2, \dots, s\}. \quad (72)$$

Repeating the similar procedure for $\mathcal{O}(\epsilon)$ terms of the mass update equation (66), we obtain,

$$\rho_{1_k}^i = \rho_{1_k}^n, \quad \text{for all } k, \quad \text{for all } i \in \{1, 2, \dots, s\}. \quad (73)$$

Since $\rho_{0,1_k}^{n+1} = \rho_{0,1_k}^s$ due to the GSA property of IMEX-RK time discretisation, we have $\rho_{0,1_k}^{n+1} = \rho_{0,1_k}^s = \rho_{0,1_k}^n$. Therefore, $\rho_{0,1_k}^n = \rho_{0,1_k}^0 \equiv \text{constant}$, for all $n = 1, 2, \dots$.

Inserting this into the $\mathcal{O}(1)$ mass and momentum update equations, we get for all $i \in \{1, 2, \dots, s\}$,

$$\sum_{j=1}^{i-1} a_{ij} D(u_{1_0})_k^j + a_{ii} D(u_{1_0})_k^n - \Delta t_n a_{ii} \sum_{j=1}^{i-1} \tilde{a}_{ij} D^2(u_{1_0})_k^j - \frac{\Delta t_n}{\rho_0} a_{ii} \sum_{j=1}^i a_{ij} D^2(p_2)_k^j = 0, \quad (74)$$

$$(u_{1_0})_k^i = (u_{1_0})_k^n - \Delta t_n \sum_{j=1}^{i-1} \tilde{a}_{ij} D_1(u_{1_0})_k^j - \frac{\Delta t_n}{\rho_0} \sum_{j=1}^i a_{ij} D_{cen}(p_2)_k^j, \quad (75)$$

where $\rho_0 = \rho_{0_k}^0 + \epsilon \rho_{1_k}^0$, for any $k = 1, 2, \dots$. □

Due to the GSA property, the expressions for $\rho_{0_k}^s, \rho_{1_k}^s, (u_{1_0})_k^s$ follow for $\rho_{0_k}^{n+1}, \rho_{1_k}^{n+1}, (u_{1_0})_k^{n+1}$, for all $k = 1, 2, \dots$. Thus, we have devised an asymptotic preserving IMEX-RK scheme with three different types of space discretisation techniques.

4 Numerical results

In this section, we present the numerical results obtained from our asymptotic preserving IMEX-RK scheme with three different types of spatial discretisation. The numerical results include: entropy, potential energy (PE), kinetic energy (KE) plots and accuracy tables of a standard periodic problem for different values of ϵ ; entropy, density and momentum plots for colliding acoustic waves and Riemann problems; entropy, PE and KE plots for Gresho and travelling vortex problems.

4.1 Standard periodic problem

The domain of the problem is $\Omega := [0, 1]$, and the initial conditions are:

$$\rho^0(x) = 1 + \epsilon^2 \sin(2\pi x) \quad (76)$$

$$u_1^0(x) = 1 + \epsilon \sin(2\pi x). \quad (77)$$

The parametric values are: $\kappa = 1$ and $\gamma = 2$. The entropy plots and accuracy tables of this problem will be presented for different values of ϵ .

4.1.1 Entropy, kinetic energy (KE) and potential energy (PE)

The domain Ω is discretised into $N = 200$ grid points. The first order IMEX scheme $ARS(1, 1, 1)$ is used along with three types of spatial discretisation techniques to obtain the plots on entropy, KE and PE. The time step is chosen as:

$$\Delta t_n = C \frac{\Delta x}{\max_{i \in \Omega_N} (u_{1i}^n)}, \quad (78)$$

where C is the CFL number, and Ω_N is the discretised set of the domain Ω (that is, $\Omega_N = \{1, 2, \dots, N\}$). Figures 1, 2 and 3 show the entropy, KE and PE plots obtained for $\epsilon = 0.5, 0.1$ and 10^{-4} respectively by using type 1, type 2 and type 3 spatial discretisation techniques. The global value of the convex entropy function at time t_n is given by

$$\eta^n = KE^n + PE^n, \text{ where } KE^n = \sum_{k=1}^N \frac{1}{2} \rho_k^n (u_{1k}^n)^2 \Delta x_k, \quad PE^n = \sum_{k=1}^N \frac{1}{\epsilon^2} \frac{p_k^n}{\gamma - 1} \Delta x_k \quad (79)$$

with $\Delta x_k = \Delta x = L/N$ for $k \in \{1, 2, \dots, N\}$, and L is the length of the domain. The plots in Figures 1, 2 and 3 are obtained at time $T = 5$ to depict the long time behaviours of entropy, KE and PE.

$\epsilon = 0.5$: From Figure 1, we observe that entropy which is the sum of kinetic and potential energies decays while kinetic and potential energies separately do not decay. It is expected as we only maintain entropy stability in the space discretisation. Such an entropy decay is observed for $C = 0.1, 0.2, \dots, 0.9$ (results corresponding to $C = 0.8$ are shown in Figure 1). The results for type 3 use $q = 0$, meaning that entropy conserving spacial discretisation is used for $\nabla \cdot (\rho \mathbf{u} \otimes \mathbf{u})$.

$\epsilon = 0.1$: Similar to $\epsilon = 0.5$, we observe for $\epsilon = 0.1$ (from Figure 2) that entropy decays while potential and kinetic energies do not. Such entropy decay is observed for $C = 0.1, 0.2, \dots, 0.9$ (results corresponding to $C = 0.8$ are shown in Figure 2). The results for type 3 are obtained with $q = 0$.

$\epsilon = 0.0001$: Unlike the previous cases, for $\epsilon = 0.0001$, the entropy decay is very sensitive to the value of C . This may be due to the entropy production from the explicit time discretisation of the nonlinear terms. The results in Figure 3 are obtained with $C = 0.5$. Further, the results for type 3 use $q = 2$, meaning that entropy stable spatial discretisation is used for $\nabla \cdot (\rho \mathbf{u} \otimes \mathbf{u})$.

4.1.2 Order of accuracy

In this subsection, we show the order of accuracy of type 2 spatial discretisation paired with $ARS(1, 1, 1)$ IMEX time discretisation that is first order accurate in time. In tables 1 and 2, we observe the order of accuracy of density ρ and velocity u_1 by using different number of grid points: $N = 20, 25, 100, 200, 500$. The reference solution is obtained with $N = 1000$. The time step is chosen according to (78) with CFL number, $C = 0.5$.

For $\epsilon = 0.5, 0.1$, both density and velocity converge with a rate of about 1. For $\epsilon = 10^{-4}$, density shows very small errors of $\mathcal{O}(10^{-7})$ for all tested values of N . This indicates that ρ_0 and ρ_1 in asymptotic expansion (11) are constant, and thus our scheme is asymptotic preserving. Further ρ_2 in asymptotic expansion (11) and the velocity u_1 are converging with a rate of about 0.5.

4.2 Colliding acoustic waves problem

The domain of the problem is $\Omega = [-1, 1]$, and the initial conditions are:

$$\rho^0(x) = 0.955 + 0.5\epsilon(1 - \cos(2\pi x)) \quad (80)$$

$$u_1^0(x) = -\text{sign}(x)\sqrt{\gamma}(1 - \cos(2\pi x)). \quad (81)$$

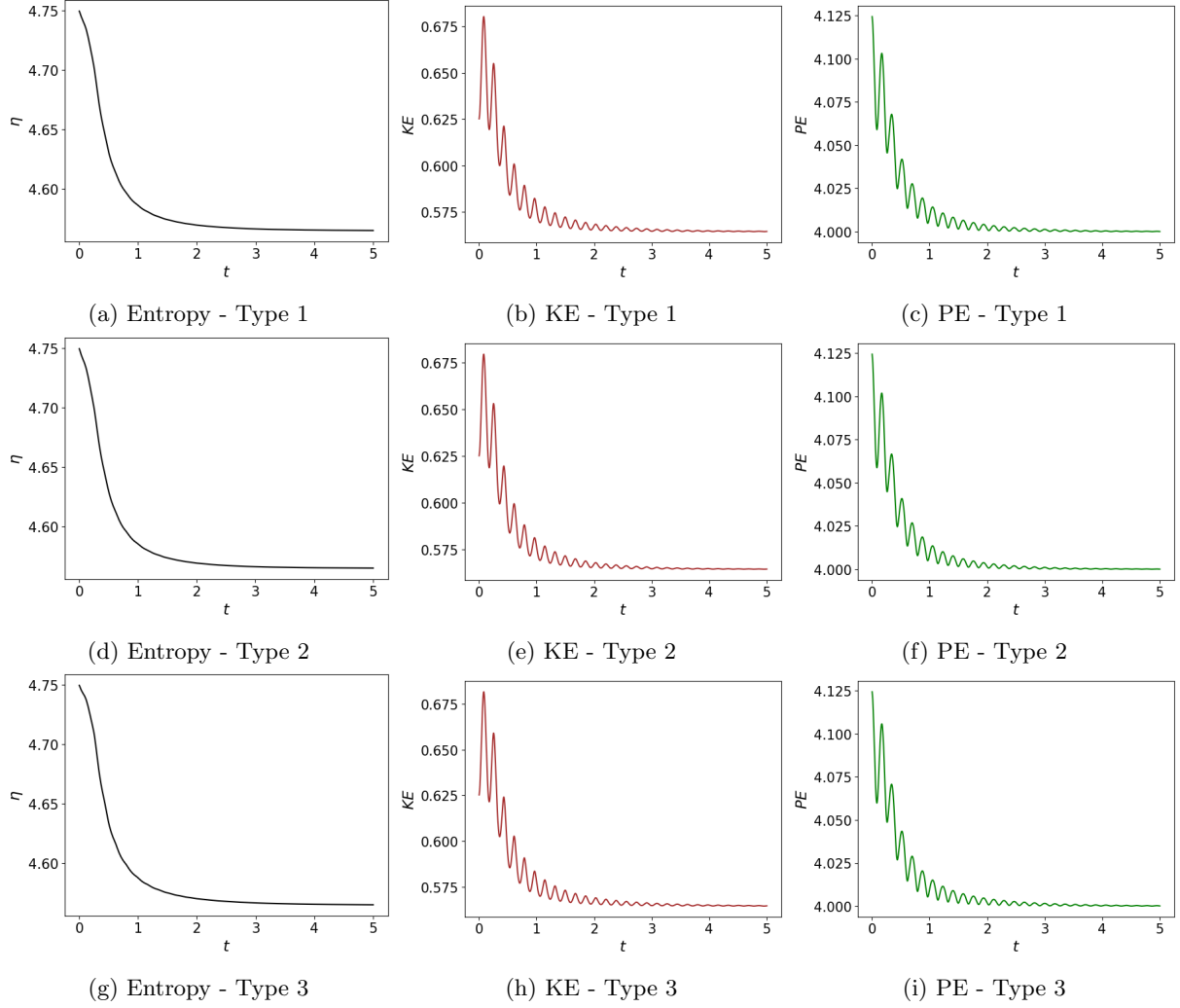


Figure 1: **Standard periodic problem:** Entropy, KE and PE plots for $\epsilon = 0.5$ using space discretisation types 1, 2 and 3

N	Δx	$\epsilon = 0.5$		$\epsilon = 0.1$		$\epsilon = 10^{-4}$	
		$\ \rho \text{ error}\ _{L_2}$	EOC	$\ \rho \text{ error}\ _{L_2}$	EOC	$\ \rho \text{ error}\ _{L_2}$	EOC
20	0.05	0.03267	-	0.00447	-	4.89×10^{-7}	-
50	0.02	0.01644	0.7497	0.00370	0.2069	4.77×10^{-7}	0.0266
100	0.01	0.01006	0.7083	0.00256	0.5315	4.52×10^{-7}	0.0773
250	0.004	0.00282	1.3874	0.00117	0.8510	3.76×10^{-7}	0.1999
500	0.002	0.00156	0.8580	0.00044	1.4177	2.49×10^{-7}	0.5962

Table 1: **Standard periodic problem:** Convergence rates of L_2 error in ρ using $ARS(1,1,1)$ coupled with type 2 discretisation.

The parametric values are: $\kappa = 1$, $\gamma = 1.4$ and $\epsilon = 0.1$. It is to be noted that the initial condition is not well-prepared. Periodic boundary conditions are used for this problem. Density and momentum plots are presented for different values of the final time $T = 0.04, 0.06, 0.08$. We also present global entropy, kinetic energy, and potential energy with respect to time. $ARS(1,1,1)$ IMEX time discretisation is used. Figures 4, 5 and 6 show the plots obtained by using type 1, type 2 and type 3 space discretisations, respectively. All three types of space discretisation result in entropy decay. While the global entropy decays, as expected, the kinetic and potential energies separately do not decay. Further, for this problem, there is no significant difference in density and momentum plots between the three types of space discretisation. The results corresponding to $C = 0.8$ are shown in Figures 4, 5, and 6. Similar entropy decay is observed for

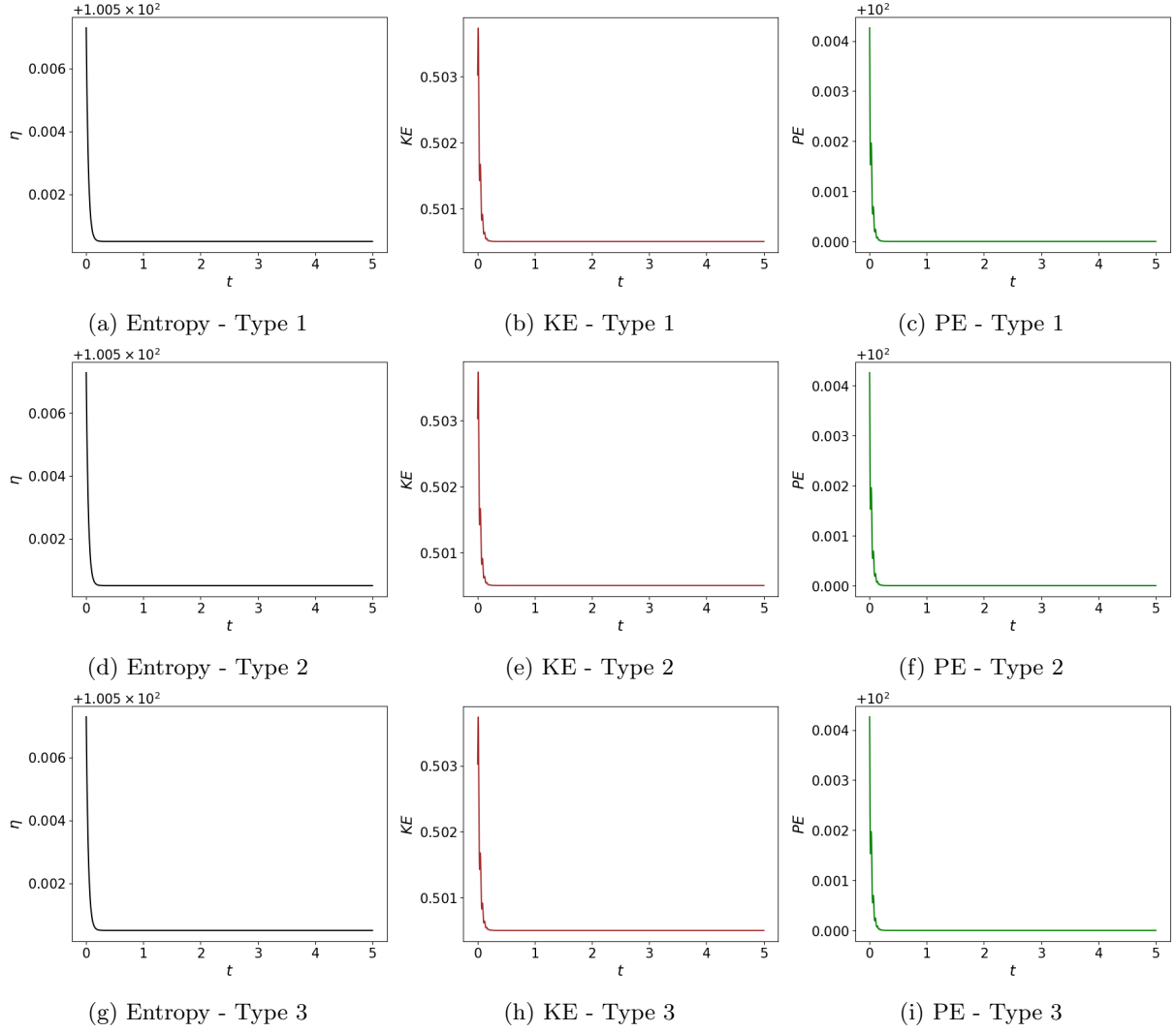


Figure 2: **Standard periodic problem:** Entropy, KE and PE plots for $\epsilon = 0.1$ using space discretisation types 1, 2 and 3

N	Δx	$\epsilon = 0.5$		$\epsilon = 0.1$		$\epsilon = 10^{-4}$	
		$\ u_1 \text{ error}\ _{L_2}$	EOC	$\ u_1 \text{ error}\ _{L_2}$	EOC	$\ u_1 \text{ error}\ _{L_2}$	EOC
20	0.05	0.12749	-	0.08749	-	5.27×10^{-7}	-
50	0.02	0.02794	0.0021	0.07201	0.2125	5.04×10^{-7}	0.0493
100	0.01	0.00628	2.1540	0.05035	0.5163	4.65×10^{-7}	0.1158
250	0.004	0.00351	0.6346	0.02121	0.9433	4.08×10^{-7}	0.1425
500	0.002	0.00127	1.4661	0.00761	1.4784	2.94×10^{-7}	0.4730

Table 2: **Standard periodic problem:** Convergence rates of L_2 error in u_1 using $ARS(1, 1, 1)$ coupled with type 2 discretisation.

$C = 0.1, 0.2, \dots, 0.9$.

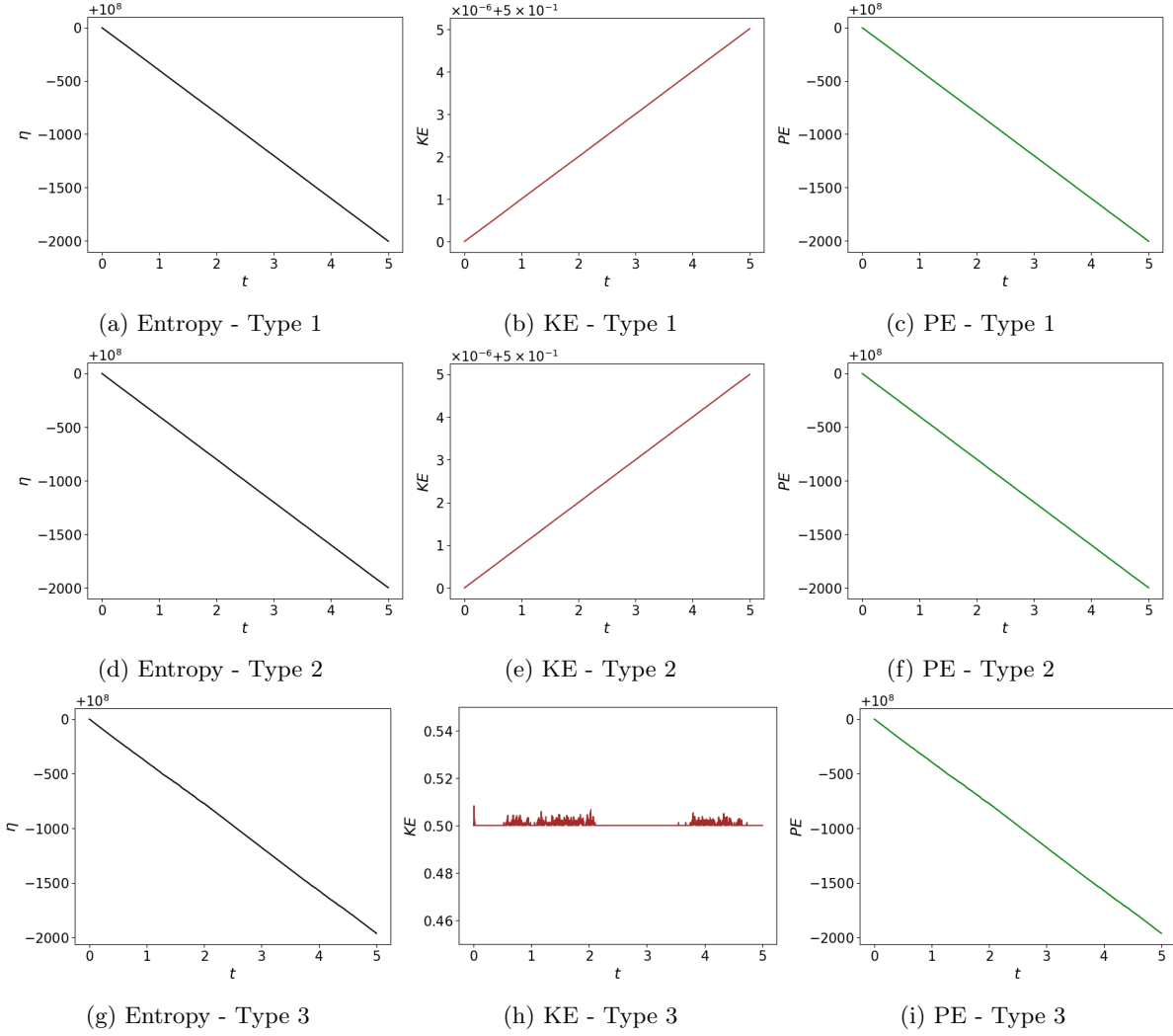


Figure 3: **Standard periodic problem:** Entropy, KE and PE plots for $\epsilon = 0.0001$ using space discretisation types 1, 2 and 3

4.3 Riemann problem

This problem is taken from [13]. The domain is $\Omega = [0, 1]$ and the initial conditions are:

$$\rho^0(x) = 1, \quad (\rho u_1)^0(x) = 1 - \epsilon^2/2, \quad \text{if } x \in [0, 0.2] \cup [0.8, 1] \quad (82)$$

$$\rho^0(x) = 1 + \epsilon^2, \quad (\rho u_1)^0(x) = 1, \quad \text{if } x \in (0.2, 0.3] \quad (83)$$

$$\rho^0(x) = 1, \quad (\rho u_1)^0(x) = 1 + \epsilon^2/2, \quad \text{if } x \in (0.3, 0.7] \quad (84)$$

$$\rho^0(x) = 1 - \epsilon^2, \quad (\rho u_1)^0(x) = 1, \quad \text{if } x \in (0.7, 0.8]. \quad (85)$$

The parametric values are: $\kappa = 1$ and $\gamma = 2$. Periodic boundary conditions are used for this problem. Density, momentum and global entropy (vs. time) plots are presented at $T = 0.05$ for different values of ϵ , such as $\epsilon = 0.8, 0.3, 0.05$. *ARS*(1, 1, 1) IMEX time discretisation is used. Figures 7, 8 and 9 show the plots obtained by using type 2, type 3 first and second order entropy stable space discretisations, respectively. Entropy decay is observed for all tested values of ϵ , while using type 2 and type 3 space discretisations. However, while type 1 space discretisation results in entropy decay for $\epsilon = 0.05, 0.3$ (figures not shown), this discretisation results in blow-up for $\epsilon = 0.8$. This is expected as type 1 space discretisation involves central discretisation of $\nabla \cdot (\rho \mathbf{u})$.

Results corresponding to $C = 0.8$ are shown for $\epsilon = 0.05, 0.3$ in Figures 7, 8 and 9. For these values of ϵ , similar entropy decay is observed when using $C = 0.1, 0.2, \dots, 0.9$. On the other hand for $\epsilon = 0.8$, $C = 0.2$ is used in Figure 7, and $C = 0.1$ is used in Figures 8 and 9.

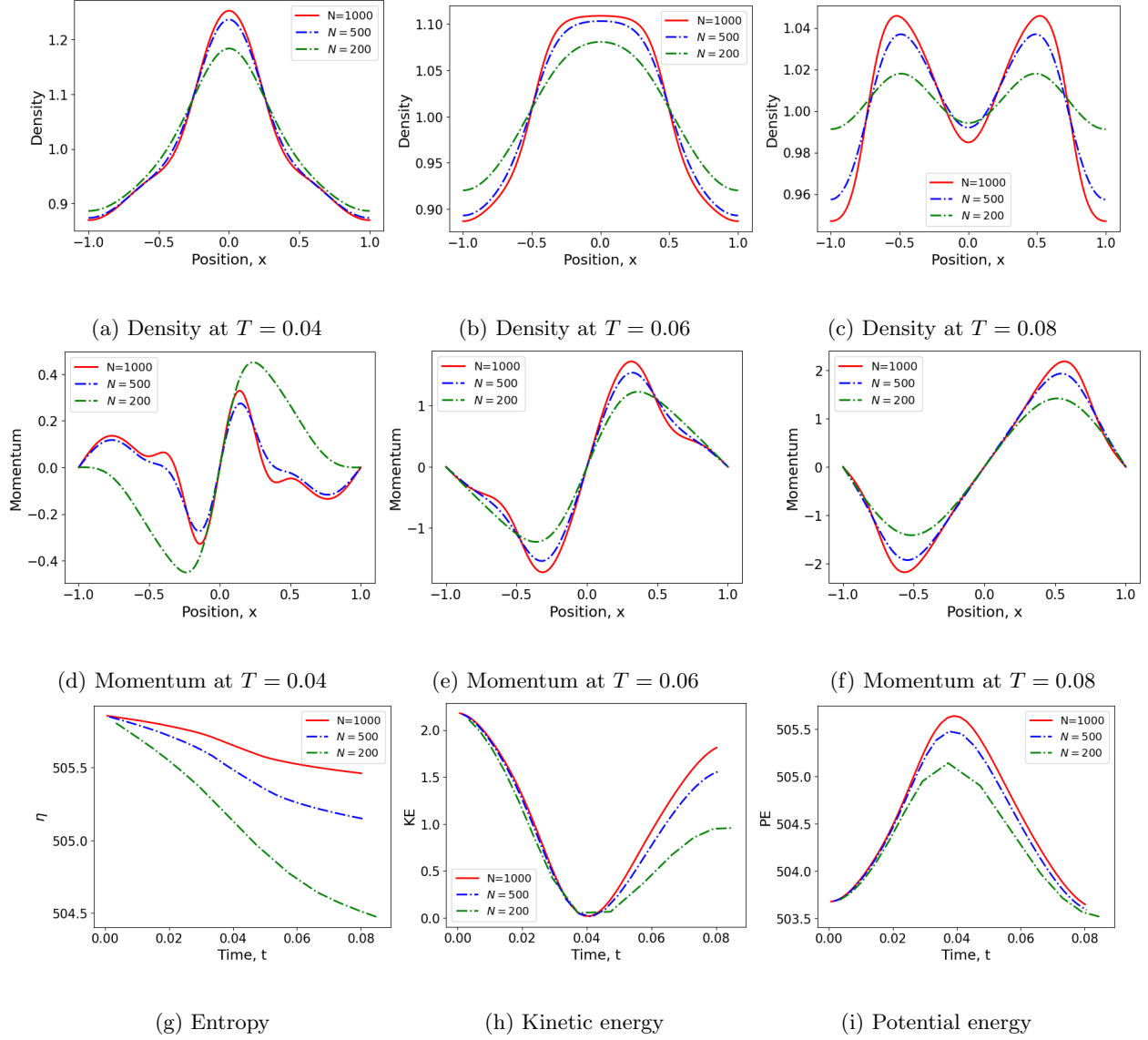


Figure 4: **Colliding acoustic waves problem** with $\epsilon = 0.1$ using type 1 space discretisation.

4.4 Gresho vortex problem

This problem is taken from [20, 33]. A vortex of radius $R = 0.4$ centered at $(x_{1_0}, x_{2_0}) = (0.5, 0.5)$ is considered at initial time $t = 0$. The initial background state is considered as: $\rho_0 = 1$, $\mathbf{u}_0 = (u_{1_0}, 0)^T$ with $u_{1_0} = 0.1$, $p_0 = 1$ and hence $a_0 = \sqrt{\frac{\gamma p_0}{\rho_0}} = \sqrt{\gamma}$.

The line velocity of the vortex is

$$u_\theta(r) = \begin{cases} 2\frac{r}{R} & \text{if } 0 \leq r < \frac{R}{2} \\ 2\left(1 - \frac{r}{R}\right) & \text{if } \frac{R}{2} \leq r < R \\ 0 & \text{if } r \geq R \end{cases},$$

and the velocity components in Cartesian coordinates are

$$u_1(x_1, x_2) = u_{1_0} - \frac{x_2 - x_{2_0}}{r} u_\theta(r), \quad u_2(x_1, x_2) = \frac{x_1 - x_{1_0}}{r} u_\theta(r).$$

Here, $r = \sqrt{(x_1 - 0.5)^2 + (x_2 - 0.5)^2}$. Upon balancing the pressure gradient and centrifugal force (*i.e.*, $\rho_0 \frac{u_\theta^2}{r} = \frac{1}{\epsilon^2} \frac{\partial p}{\partial r}$), pressure is derived as:

$$p(r) = p_0 + \epsilon^2 \begin{cases} 2\frac{r^2}{R^2} + 2 - \log 16 & \text{if } 0 \leq r < \frac{R}{2} \\ 2\frac{r^2}{R^2} - 8\frac{r}{R} + 4\log\left(\frac{r}{R}\right) + 6 & \text{if } \frac{R}{2} \leq r < R \\ 0 & \text{if } r \geq R \end{cases}.$$

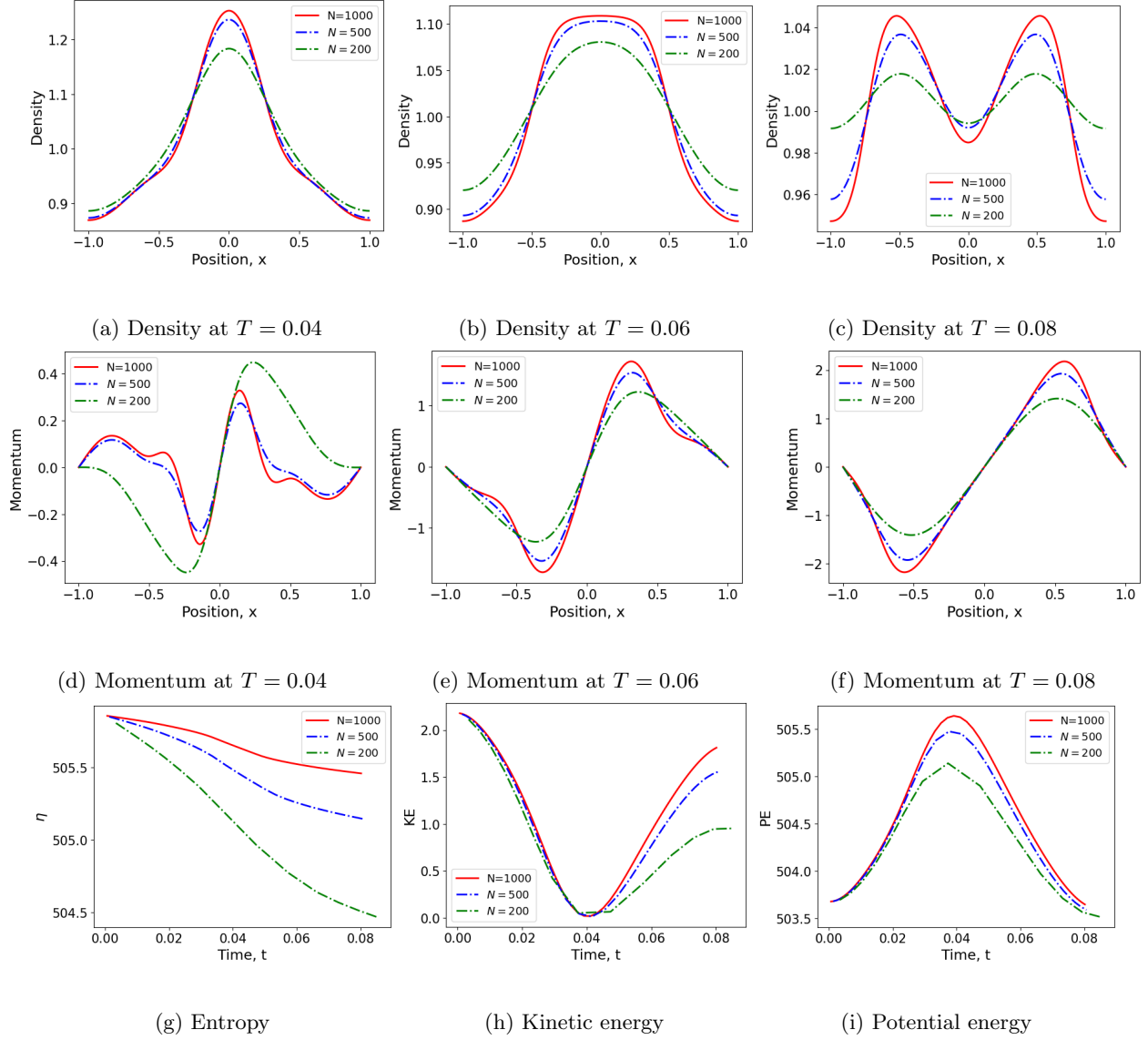


Figure 5: **Colliding acoustic waves problem** with $\epsilon = 0.1$ using type 2 space discretisation.

We assume adiabatic compression $p = \rho^\gamma$ with $\gamma = 1.4$, and use asymptotic expansion: $p = p_0 + \epsilon^2 p_2$, $\rho = \rho_0 + \epsilon^2 \rho_2$. Comparing $\frac{\partial p}{\partial \epsilon} = 2\epsilon p_2$ and $\frac{\partial p}{\partial \epsilon} = \frac{\partial p}{\partial \rho} \frac{\partial \rho}{\partial \epsilon} = \frac{\gamma p}{\rho} 2\epsilon \rho_2$, we obtain $\rho_2 = \frac{p_2}{\gamma}$ by noting that $p = 1, \rho = 1$ up to the leading order. ρ_2 can then be used to evaluate ρ as $\rho = \rho_0 + \epsilon^2 \rho_2$. Periodic boundary conditions are imposed in both directions. The problem is simulated using *ARS*(1, 1, 1) IMEX time discretisation and type 2 space discretisation for $\epsilon = 0.1, 0.01, 0.001$. The following quantities are observed:

$$\eta = 1/2 \rho(u_1^2 + u_2^2) + (1/\epsilon^2)p/(\gamma - 1), \quad \text{PE} = (1/\epsilon^2)p/(\gamma - 1), \quad (86)$$

$$\text{KE} = \frac{1}{2} ((u_1 - u_{10})^2 + u_2^2) \quad \text{where } u_{10} \text{ is the background velocity} \quad (87)$$

$$\text{Mach number ratio, } M_{\text{ratio}} = \left(\sqrt{\frac{(u_1 - u_{10})^2 + u_2^2}{\gamma p / \rho}} \right). \quad (88)$$

Figure 10 shows the evolution of entropy (η), KE and PE over time upto $T = R\pi$. A CFL value of $C = 0.5$ is used for $\epsilon = 0.1, 0.01, 0.001$. As expected, the entropy and kinetic energy are decaying in time, although the potential energy separately does not decay. Figure 11 shows the contours of M_{ratio} at $T = R\pi$. Tables 3 to 5 show the convergence rates of ρ, u_1 and u_2 for $\epsilon = 0.1, 0.01$ and 0.001 . It is observed that the required convergence rate is obtained for all the values of ϵ .

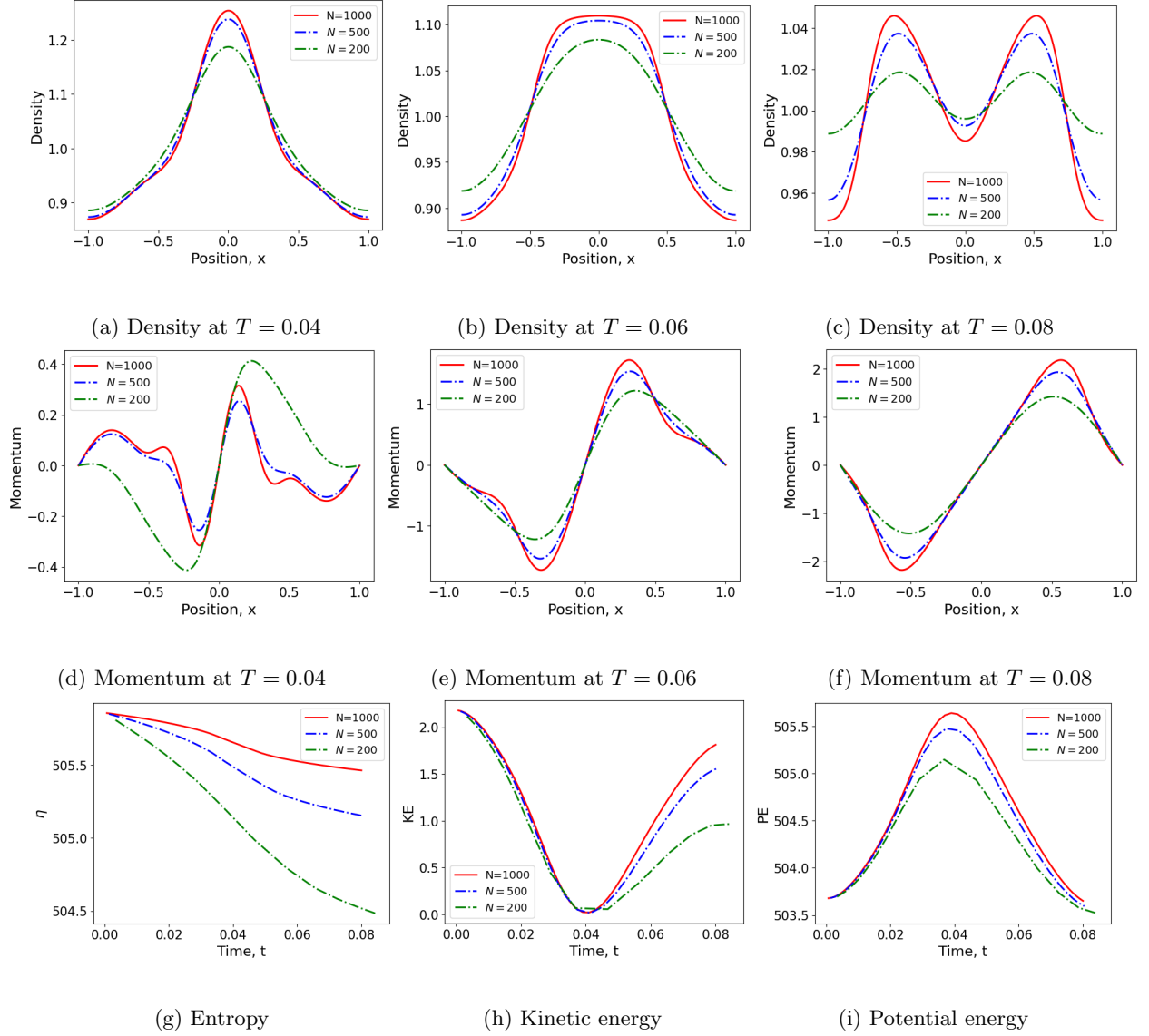


Figure 6: **Colliding acoustic waves problem** with $\epsilon = 0.1$ using type 3 space discretisation.

N	$\epsilon = 10^{-1}$		$\epsilon = 10^{-2}$		$\epsilon = 10^{-3}$	
	$\ \rho \text{ error}\ _{L_2}$	EOC	$\ \rho \text{ error}\ _{L_2}$	EOC	$\ \rho \text{ error}\ _{L_2}$	EOC
10	0.00084239	-	$8.42982872 \times 10^{-6}$	-	$8.45384875 \times 10^{-8}$	-
20	0.00058693	0.4836	$5.87421133 \times 10^{-6}$	0.4834	$5.90367676 \times 10^{-8}$	0.4805
25	0.00050582	0.6367	$5.06282663 \times 10^{-6}$	0.6363	$5.10971760 \times 10^{-8}$	0.6182
50	0.00023863	1.0525	$2.38934881 \times 10^{-6}$	1.0520	$2.56732036 \times 10^{-8}$	0.9643

Table 3: **Gresho vortex problem**: Convergence rates of L_2 error in ρ using $ARS(1, 1, 1)$ coupled with type 2 discretisation

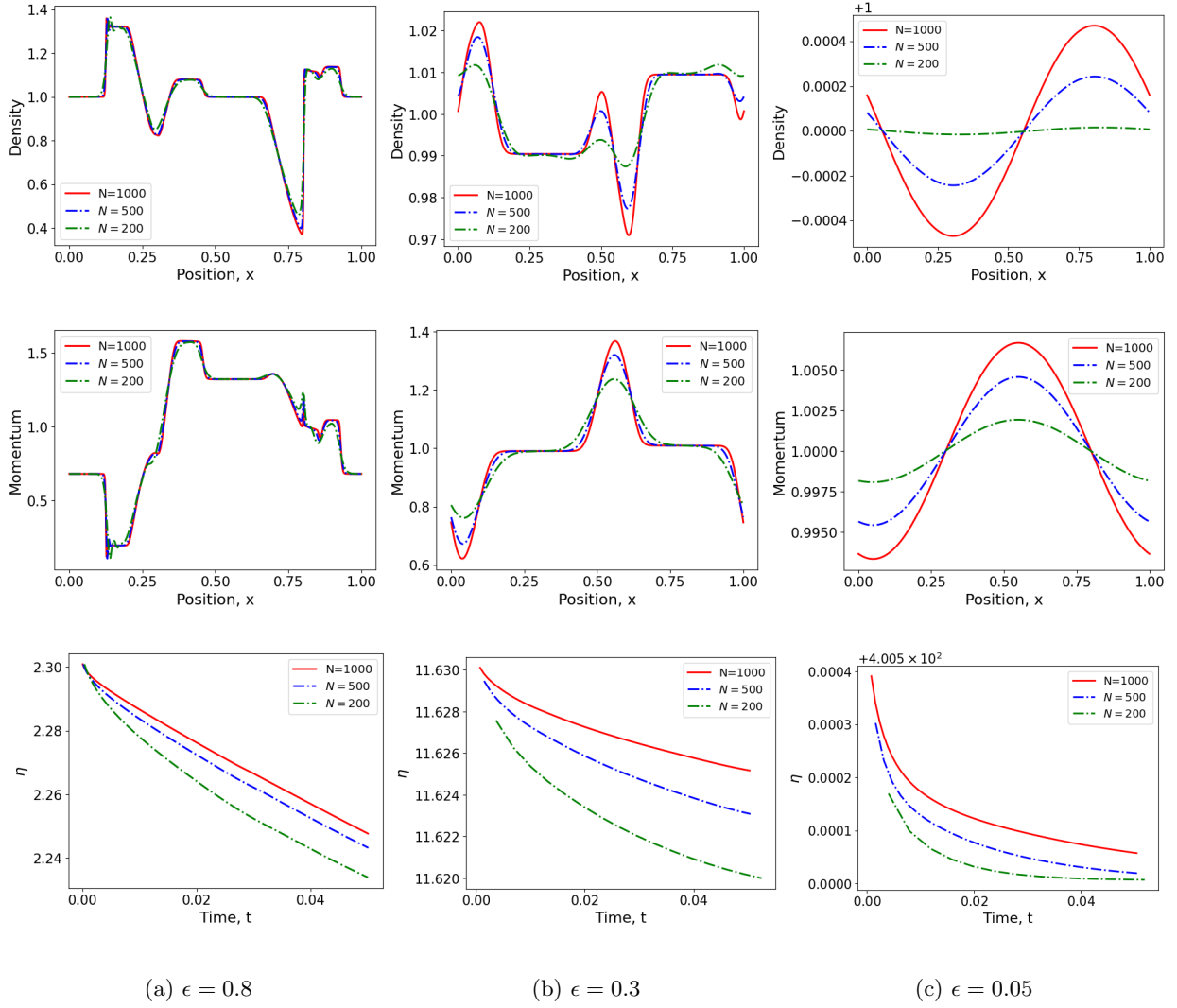


Figure 7: **Riemann problem** at $T = 0.05$ using type 2 space discretisation.

N	$\epsilon = 10^{-1}$		$\epsilon = 10^{-2}$		$\epsilon = 10^{-3}$	
	$\ u_1 \text{ error}\ _{L_2}$	EOC	$\ u_1 \text{ error}\ _{L_2}$	EOC	$\ u_1 \text{ error}\ _{L_2}$	EOC
10	0.17944234	-	0.179428512	-	0.179428376	-
20	0.105626	0.7092	0.105625341	0.7091	0.105625335	0.7091
25	0.08712198	0.8244	0.0871283562	0.8241	0.0871284204	0.8241
50	0.0367448	1.2095	0.0367560804	1.2092	0.0367561927	1.2092

Table 4: **Gresho vortex problem**: Convergence rates of L_2 error in u_1 using $ARS(1, 1, 1)$ coupled with type 2 discretisation

4.5 Travelling vortex problem

The travelling vortex problem taken from [5] is considered here for the isentropic Euler system with $p = \rho^{1.4}$. The initial condition for the problem is given by,

$$\rho^0(x_1, x_2) = 110 + \epsilon^2 \left(\frac{1.5}{4\pi} \right)^2 D(x_1, x_2) (k(r) - k(\pi)) \quad (89)$$

$$u_1^0(x_1, x_2) = 0.6 + 1.5(1 + \cos(r(x_1, x_2))) D(x_1, x_2) (0.5 - x_2) \quad (90)$$

$$u_2^0(x_1, x_2) = 0 + 1.5(1 + \cos(r(x_1, x_2))) D(x_1, x_2) (x_1 - 0.5) \quad (91)$$

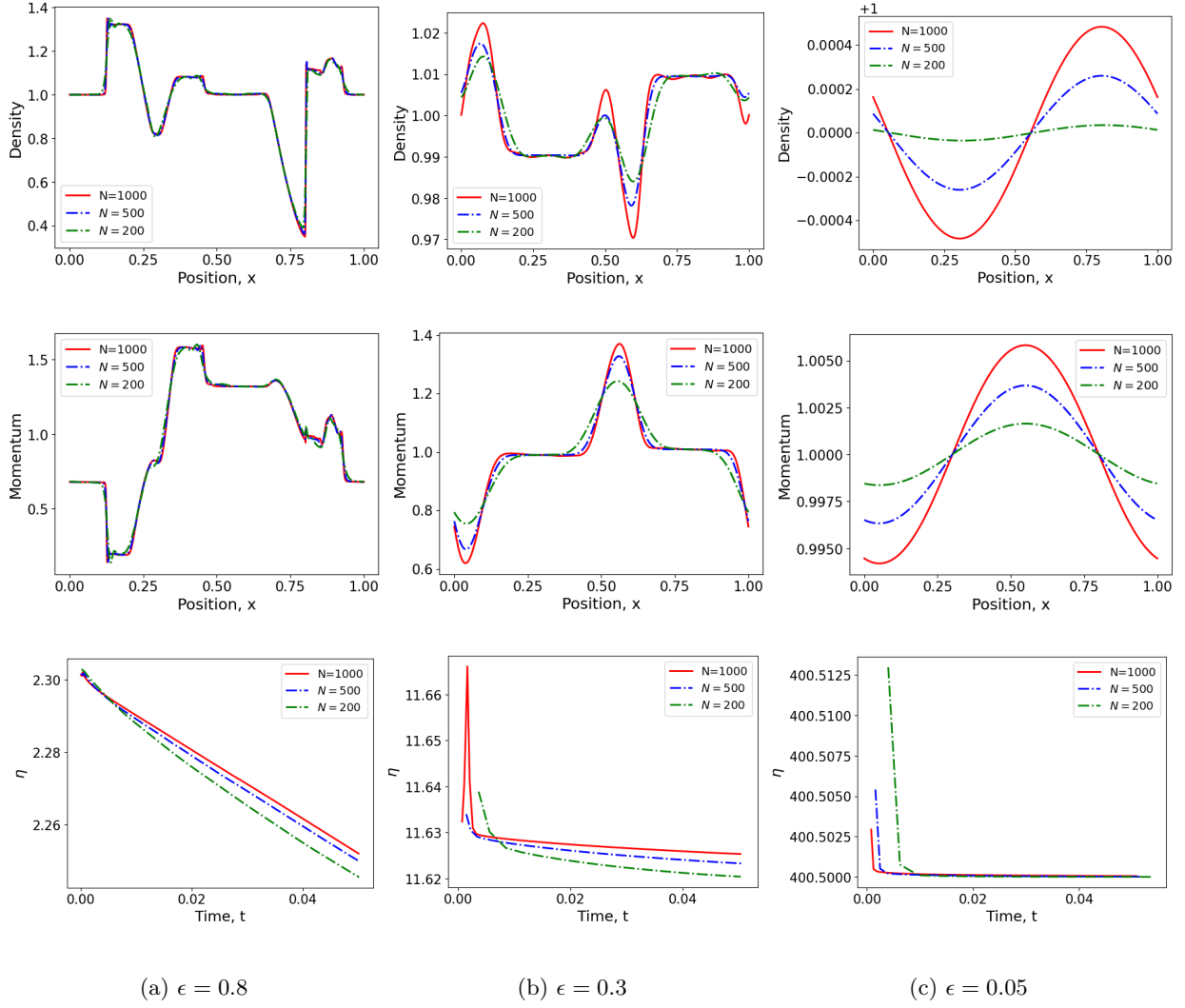


Figure 8: **Riemann problem** at $T = 0.05$ using 1^{st} order type 3 space discretisation with $q = 1$.

N	$\epsilon = 10^{-1}$		$\epsilon = 10^{-2}$		$\epsilon = 10^{-3}$	
	$\ u_2 \text{ error}\ _{L_2}$	EOC	$\ u_2 \text{ error}\ _{L_2}$	EOC	$\ u_2 \text{ error}\ _{L_2}$	EOC
10	0.1882019	-	0.188182499	-	0.188182305	-
20	0.11598214	0.64784505	0.115974954	0.6478	0.115974882	0.6478
25	0.0951939	0.84549546	0.0951936708	0.8452	0.0951936685	0.8452
50	0.04058436	1.1944146	0.0405921055	1.1941	0.0405921819e	1.194

Table 5: **Gresho vortex problem**: Convergence rates of L_2 error in u_2 using $ARS(1, 1, 1)$ coupled with type 2 discretisation

with

$$k(q) = 2 \cos(q) + 2q \sin(q) + \frac{1}{8} \cos(2q) + \frac{1}{4} q \sin(2q) + \frac{3}{4} q^2 \quad (92)$$

$$r(x_1, x_2) = 4\pi \left((x_1 - 0.5)^2 + (x_2 - 0.5)^2 \right)^{\frac{1}{2}} \quad (93)$$

$$D(x_1, x_2) = \begin{cases} 1 & \text{if } r(x_1, x_2) < \pi \\ 0 & \text{otherwise} \end{cases} \quad (94)$$

The boundary is periodic, and the domain of the problem is $[0, 1] \times [0, 1]$. Figure 12 shows the evolution of entropy (η), KE and PE over time upto $T = 1/0.6$ (which is the time period for the vortex to return to its initial position) for different values of ϵ . A CFL value of $C = 0.6$ is used for all the values of ϵ that are

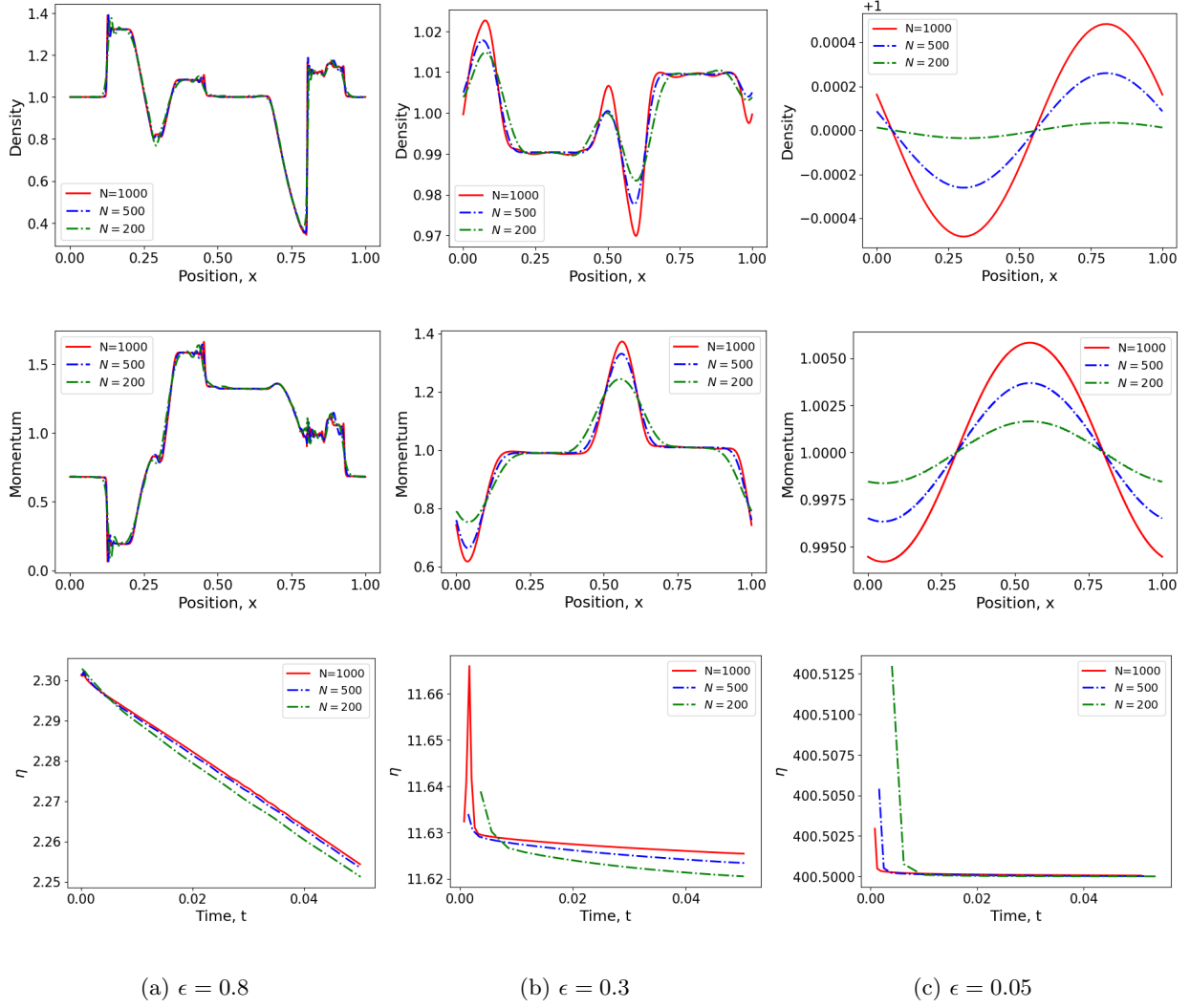


Figure 9: **Riemann problem** at $T = 0.05$ using 2^{nd} order type 3 space discretisation with $q = 1$.

considered. As expected, the entropy and kinetic energy are decaying in time, although the potential energy separately does not decay. Figure 13 shows the contours of density at $T = 1/0.6$.

Tables 6 to 9 show the convergence rates of u_1 and u_2 for $\epsilon = 10^{-1}, 10^{-2}, 10^{-3}, 10^{-4}, 10^{-5}, 10^{-6}$. It is observed that the required convergence rate is obtained for all the values of ϵ .

N	$\epsilon = 10^{-1}$		$\epsilon = 10^{-2}$		$\epsilon = 10^{-3}$	
	$\ u_1 \text{ error}\ _{L_2}$	EOC	$\ u_1 \text{ error}\ _{L_2}$	EOC	$\ u_1 \text{ error}\ _{L_2}$	EOC
10	2.53×10^{-2}	-	2.53×10^{-2}	-	2.53×10^{-2}	-
20	1.48×10^{-2}	0.71	1.48×10^{-2}	0.71	1.48×10^{-2}	0.71
25	1.24×10^{-2}	0.75	1.24×10^{-2}	0.75	1.24×10^{-2}	0.75
50	5.71×10^{-3}	1.09	5.71×10^{-3}	1.09	5.71×10^{-3}	1.09

Table 6: **Travelling vortex problem:** Convergence rates of L_2 error in u_1 using $ARS(1,1,1)$ coupled with type 2 discretisation

5 Summary and Conclusions

In this paper, we have derived and analysed entropy stable methods in the low Mach number regime. First, an entropy inequality corresponding to convex entropy function depending on Mach number ϵ is derived for the

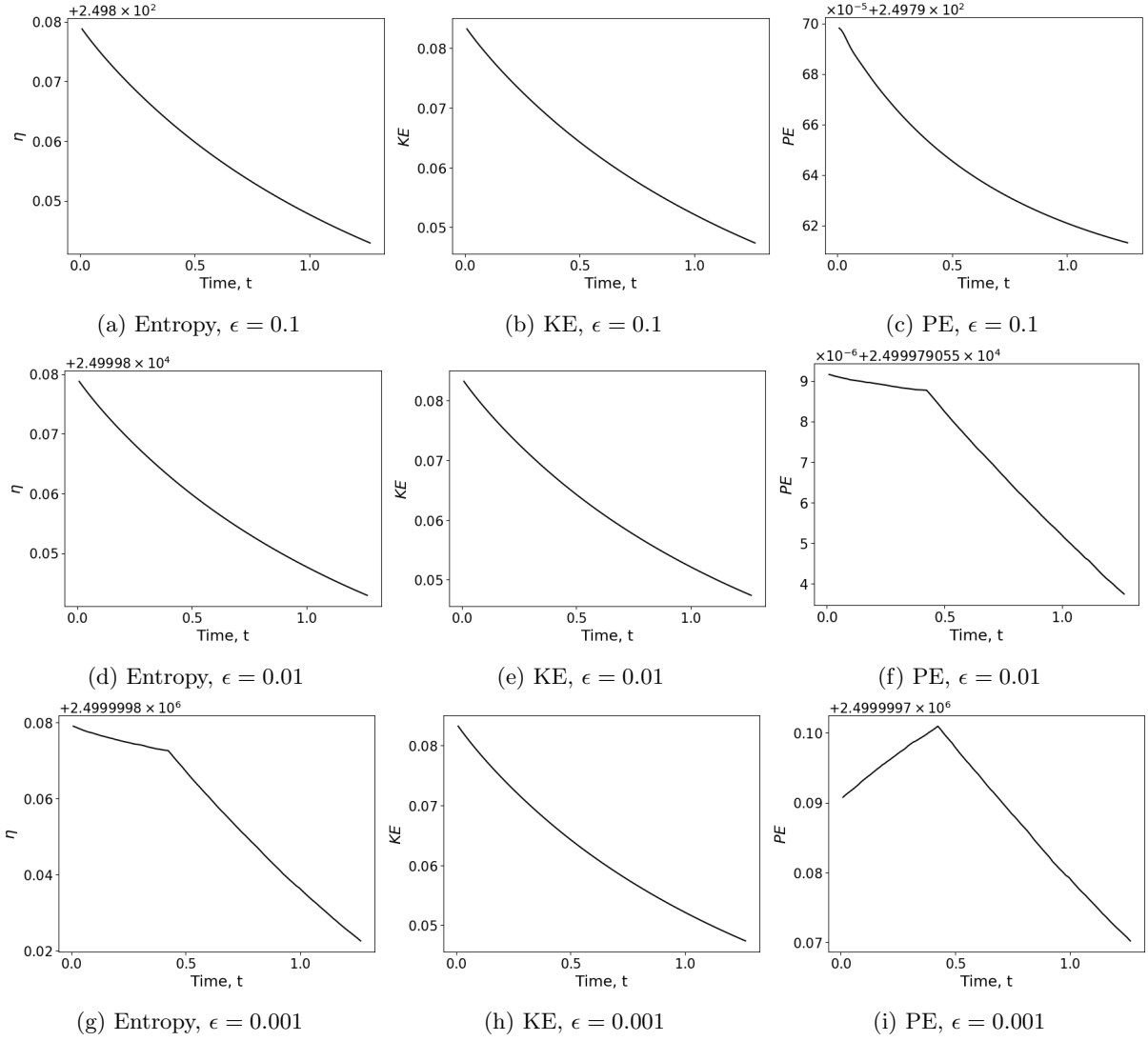


Figure 10: **Gresho vortex problem:** Entropy, KE and PE plots using space discretisation type 2 for $\epsilon = 0.1, 0.01, 0.001$ on 50×50 grid

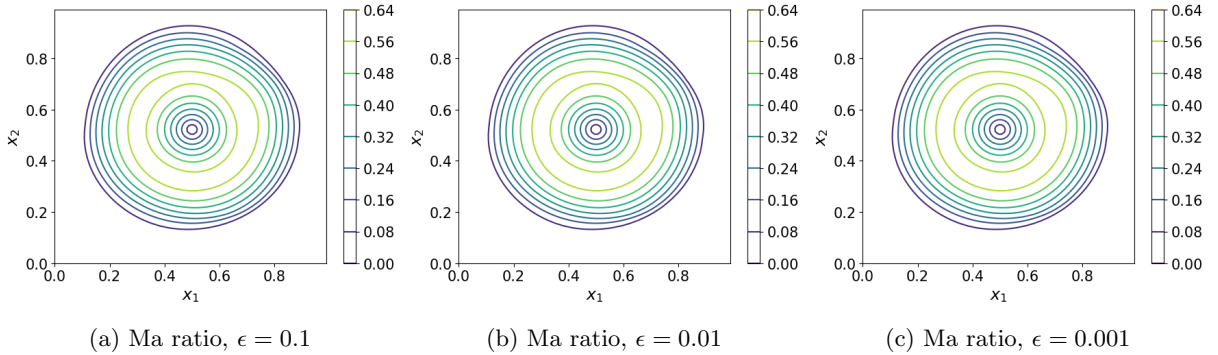


Figure 11: **Gresho vortex problem:** Ma ratio plots using space discretisation type 2 for $\epsilon = 0.1, 0.01, 0.001$ on 100×100 grid

barotropic Euler system. Then, in order to accurately and efficiently approximate low Mach number regimes in the barotropic Euler system, the IMEX-type discretisation in time is combined with a suitable entropy stable discretisation in space yielding asymptotic preserving methods. We have proposed three strategies for discretisation in space and analysed them with respect to accuracy and entropy stability. Numerical experiments confirm entropy stable approximation in the low Mach number regime.

N	$\epsilon = 10^{-4}$		$\epsilon = 10^{-5}$		$\epsilon = 10^{-6}$	
	$\ \mathbf{u}_1 \text{ error}\ _{L_2}$	EOC	$\ \mathbf{u}_1 \text{ error}\ _{L_2}$	EOC	$\ \mathbf{u}_1 \text{ error}\ _{L_2}$	EOC
10	2.53×10^{-2}	-	2.53×10^{-2}	-	8.74×10^{-2}	-
20	1.48×10^{-2}	0.71	1.48×10^{-2}	0.71	5.27×10^{-2}	0.68
25	1.24×10^{-2}	0.75	1.24×10^{-2}	0.75	4.57×10^{-2}	0.61
50	5.71×10^{-3}	1.09	5.71×10^{-3}	1.09	2.06×10^{-2}	1.12

Table 7: **Travelling vortex problem:** Convergence rates of L_2 error in u_1 using $ARS(1, 1, 1)$ coupled with type 2 discretisation

N	$\epsilon = 10^{-1}$		$\epsilon = 10^{-2}$		$\epsilon = 10^{-3}$	
	$\ \mathbf{u}_2 \text{ error}\ _{L_2}$	EOC	$\ \mathbf{u}_2 \text{ error}\ _{L_2}$	EOC	$\ \mathbf{u}_2 \text{ error}\ _{L_2}$	EOC
10	2.32×10^{-2}	-	2.32×10^{-2}	-	2.32×10^{-2}	-
20	1.71×10^{-2}	0.41	1.71×10^{-2}	0.41	1.71×10^{-2}	0.41
25	1.51×10^{-2}	0.55	1.51×10^{-2}	0.55	1.51×10^{-2}	0.55
50	7.69×10^{-3}	0.94	7.69×10^{-3}	0.94	7.69×10^{-3}	0.94

Table 8: **Travelling vortex problem:** Convergence rates of L_2 error in u_2 using $ARS(1, 1, 1)$ coupled with type 2 discretisation

N	$\epsilon = 10^{-4}$		$\epsilon = 10^{-5}$		$\epsilon = 10^{-6}$	
	$\ \mathbf{u}_2 \text{ error}\ _{L_2}$	EOC	$\ \mathbf{u}_2 \text{ error}\ _{L_2}$	EOC	$\ \mathbf{u}_2 \text{ error}\ _{L_2}$	EOC
10	2.32×10^{-2}	-	2.31×10^{-2}	-	2.19×10^{-2}	-
20	1.71×10^{-2}	0.41	1.71×10^{-2}	0.41	1.93×10^{-2}	0.17
25	1.51×10^{-2}	0.55	1.50×10^{-2}	0.55	1.88×10^{-2}	0.10
50	7.69×10^{-3}	0.94	7.76×10^{-3}	0.92	1.32×10^{-2}	0.49

Table 9: **Travelling vortex problem:** Convergence rates of L_2 error in u_2 using $ARS(1, 1, 1)$ coupled with type 2 discretisation

A Appendix: Butcher tableau

The first order type CK-ARS double Butcher tableau (known as $ARS(1, 1, 1)$) is:

$$\begin{array}{c|cc} 0 & 0 & 0 \\ 1 & 1 & 0 \\ \hline & 1 & 0 \end{array} \quad \begin{array}{c|cc} 0 & 0 & 0 \\ 1 & 0 & 1 \\ \hline & 0 & 1 \end{array} \quad (95)$$

The following is the 2-stage second order accurate Butcher tableau $ARS(2, 2, 2)$:

$$\begin{array}{c|ccc} 0 & 0 & 0 & 0 \\ \gamma & \gamma & 0 & 0 \\ 1 & \delta & 1-\delta & 0 \\ \hline & \delta & 1-\delta & 0 \end{array} \quad \begin{array}{c|ccc} 0 & 0 & 0 & 0 \\ \gamma & 0 & \gamma & 0 \\ 1 & 0 & 1-\gamma & \gamma \\ \hline & 0 & 1-\gamma & \gamma \end{array}$$

Here, $\gamma = 1 - \frac{1}{\sqrt{2}}$ and $\delta = 1 - \frac{1}{2\gamma}$.

Acknowledgements

The authors thank Hendrik Ranocha (Mainz) and Arpit Babbar (Mainz) for fruitful discussions on this topic.

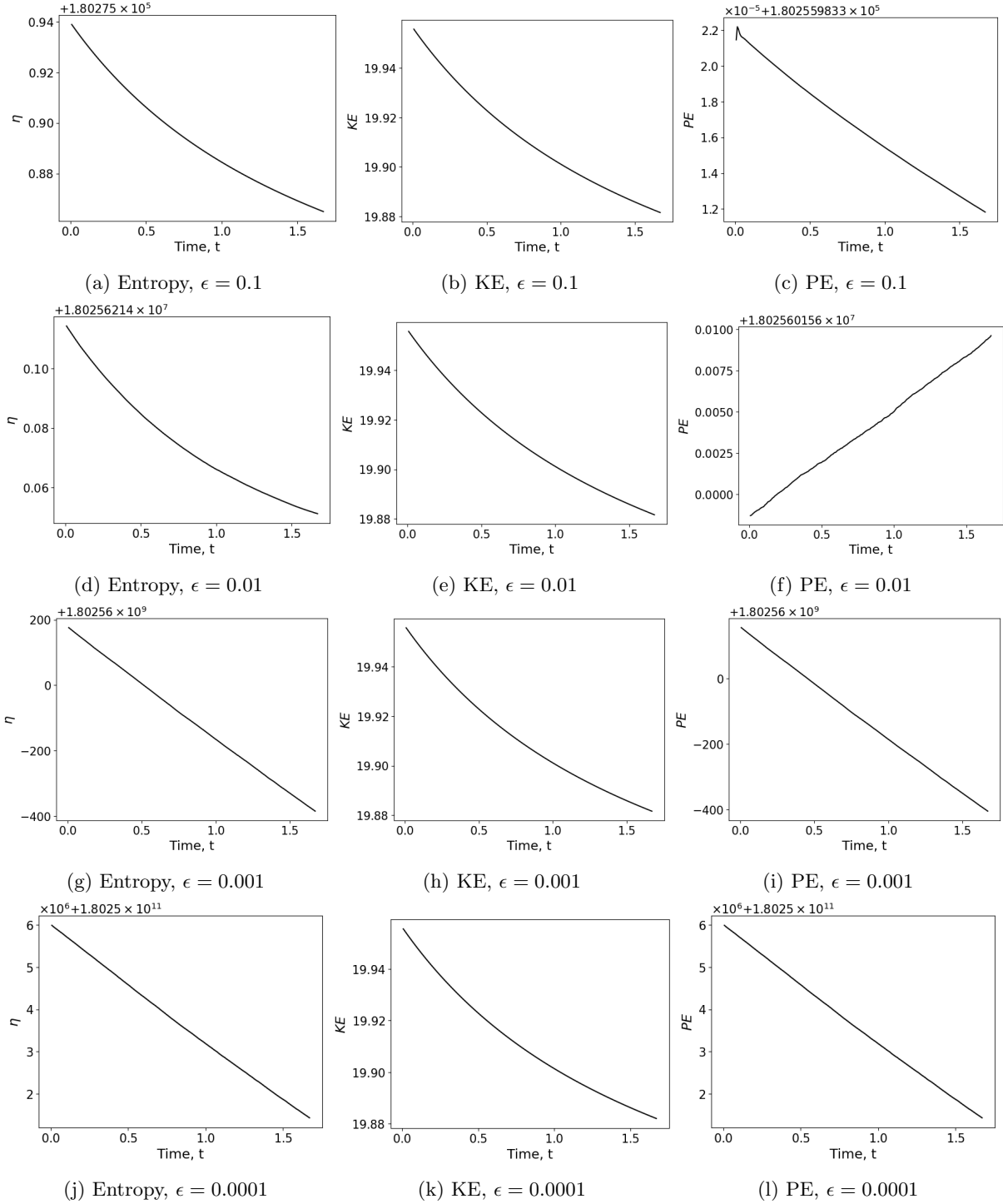


Figure 12: **Travelling vortex problem:** Entropy, KE and PE plots using space discretisation type 2 for $\epsilon = 0.1, 0.01, 0.001$ on 100×100 grid

References

- [1] M. Anandan and S. V. Raghurama Rao. Entropy conserving/stable schemes for a vector-kinetic model of hyperbolic systems. *Appl. Math. Comput.*, 465:128410, 2024.
- [2] K. R. Arun and S. Samantaray. Asymptotic preserving low Mach number accurate IMEX finite volume schemes for the isentropic Euler equations. *J. Sci. Comput.*, 82(35), 2020.
- [3] T. Barth. Numerical methods for gasdynamic systems on unstructured systems. In M. O. D. Kröner and C. Rohde, editors, *An introduction to recent developments in theory and numerics for conservation*

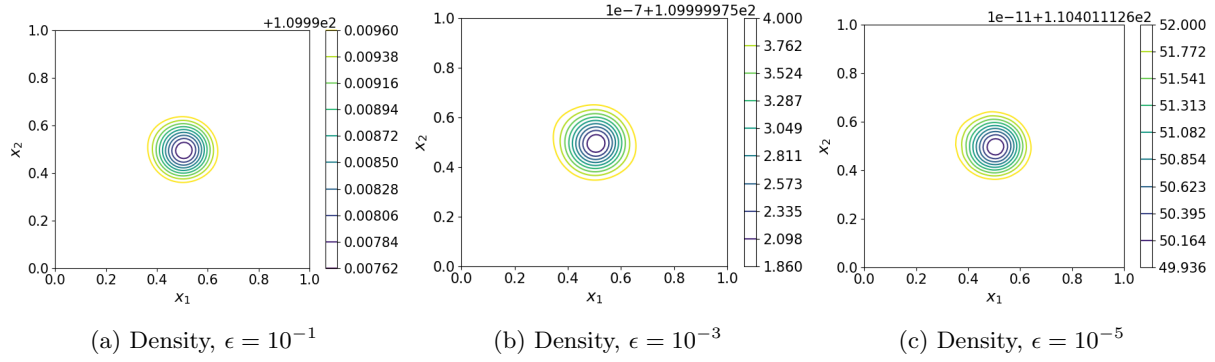


Figure 13: **Travelling vortex problem:** Density contours using space discretisation type 2 for $\epsilon = 10^{-1}, 10^{-3}, 10^{-5}$ on 100×100 grid

laws, pages 195–285. Springer, Berlin, 1999.

- [4] G. Bispen, K. R. Arun, M. Lukáčová-Medvid'ová, and S. Noelle. IMEX large time step finite volume methods for low Froude number shallow water flows. *Commun. Comput. Phys.*, 16(2):307–347, 2014.
- [5] G. Bispen, M. Lukáčová-Medvid'ová, and L. Yelash. Asymptotic preserving IMEX finite volume schemes for low Mach number Euler equations with gravitation. *J. Comput. Phys.*, 335:222–248, 2017.
- [6] S. Boscarino, J.-M. Qiu, G. Russo, and T. Xiong. A high order semi-implicit IMEX WENO scheme for the all-Mach isentropic Euler system. *J. Comput. Phys.*, 392:594–618, 2019.
- [7] S. Boscarino, G. Russo, and L. Scandurra. All Mach number second order semi-implicit scheme for the Euler equations of gas dynamics. *J. Sci. Comput.*, 77:850–884, 2018.
- [8] P. Chandrashekar. Kinetic energy preserving and entropy stable finite volume schemes for compressible Euler and Navier-Stokes equations. *Commun. Comput. Phys.*, 14(5):1252–1286, 2013.
- [9] P. Chandrashekar and C. Klingenberg. Entropy stable finite volume scheme for ideal compressible MHD on 2-D cartesian meshes. *SIAM J. Numer. Anal.*, 54(2):1313–1340, 2016.
- [10] H. Chizari, V. Singh, and F. Ismail. Cell-vertex entropy-stable finite volume methods for the system of Euler equations on unstructured grids. *Comput. Math. Appl.*, 98:261–279, 2021.
- [11] F. Corder, P. Degond, and A. Kumbaro. An asymptotic-preserving all-speed scheme for the Euler and Navier-Stokes equations. *J. Comput. Phys.*, 231(17):5685–5704, 2012.
- [12] J. Crean, J. E. Hicken, D. C. Del Rey Fernández, D. W. Zingg, and M. H. Carpenter. Entropy-stable summation-by-parts discretization of the Euler equations on general curved elements. *J. Comput. Phys.*, 356:410–438, 2018.
- [13] P. Degond and M. Tang. All speed scheme for the low Mach number limit of the isentropic Euler equations. *Commun. Comput. Phys.*, 10(1):1–31, 2011.
- [14] S. Dellacherie. Analysis of Godunov type schemes applied to the compressible Euler system at low Mach number. *J. Comput. Phys.*, 229(4):978–1016, 2010.
- [15] G. Dimarco, R. Loubère, and M.-H. Vignal. Study of a new asymptotic preserving scheme for the Euler system in the low Mach number limit. *SIAM J. Sci. Comput.*, 39(5):A2099–A2128, 2017.
- [16] G. Dimarco, R. Loubère, V. Michel-Dansac, and M.-H. Vignal. Second-order implicit-explicit total variation diminishing schemes for the Euler system in the low Mach regime. *J. Comput. Phys.*, 372:178–201, 2018.
- [17] U. S. Fjordholm, S. Mishra, and E. Tadmor. Arbitrarily high-order accurate entropy stable essentially nonoscillatory schemes for systems of conservation laws. *SIAM J. Numer. Anal.*, 50(2):544–573, 2012.
- [18] G. J. Gassner, A. R. Winters, and D. A. Kopriva. A well balanced and entropy conservative discontinuous Galerkin spectral element method for the shallow water equations. *Appl. Math. Comput.*, 272:291–308, 2016.

- [19] G. J. Gassner, A. R. Winters, and D. A. Kopriva. Split form nodal discontinuous Galerkin schemes with summation-by-parts property for the compressible Euler equations. *J. Comput. Phys.*, 327:39–66, 2016.
- [20] P. M. Gresho and S. T. Chan. On the theory of semi-implicit projection methods for viscous incompressible flow and its implementation via a finite element method that also introduces a nearly consistent mass matrix. Part 2: Implementation. *Int. J. Numer. Meth. Fl.*, 11(5):621–659, 1990.
- [21] J. Haack, S. Jin, and J. Liu. An all-speed asymptotic-preserving method for the isentropic Euler and Navier-Stokes equations. *Commun. Comput. Phys.*, 12(4):955–980, 2012.
- [22] F. Ismail and P. L. Roe. Affordable, entropy-consistent Euler flux functions II: Entropy production at shocks. *J. Comput. Phys.*, 228(15):5410–5436, 2009.
- [23] S. Jin. Efficient asymptotic-preserving (AP) schemes for some multiscale kinetic equations. *SIAM J. Sci. Comput.*, 21:441–454, 1999.
- [24] S. Jin. Asymptotic preserving (AP) schemes for multiscale kinetic and hyperbolic equations: a review. *Riv. Mat. Univ. Parma*, pages 177–216, 2012.
- [25] S. Klainerman and A. Majda. Singular limits of quasilinear hyperbolic systems with large parameters and the incompressible limit of compressible fluids. *Commun. Pur. Appl. Math.*, 34(4):481–524, 1981.
- [26] S. Klainerman and A. Majda. Compressible and incompressible fluids. *Commun. Pur. Appl. Math.*, 35(5):629–651, 1982.
- [27] S. Noelle, G. Bispen, K. R. Arun, M. Lukáčová-Medviďová, and C.-D. Munz. A weakly asymptotic preserving low Mach number scheme for the Euler equations of gas dynamics. *SIAM J. Sci. Comput.*, 36(6):B989–B1024, 2014.
- [28] M. Parisot. Entropy-satisfying scheme for a hierarchy of dispersive reduced models of free surface flow. *Int. J. Numer. Meth. Fl.*, 91(10):509–531, 2019.
- [29] G. Puppo and M. Semplice. Entropy and the numerical integration of conservation laws. In *Proceedings of the 2nd Annual Meeting of the Lebanese Society for Mathematical Sciences (LSMS-2011)*, 2011.
- [30] G. Puppo and M. Semplice. Numerical entropy and adaptivity for finite volume schemes. *Commun. Comput. Phys.*, 10(5):1132–1160, 2011.
- [31] D. Ray and P. Chandrashekar. Entropy stable schemes for compressible Euler equations. *Int. J. Numer. Anal. Mod.*, 4(4):335 – 352, 2013.
- [32] D. Ray, P. Chandrashekar, U. S. Fjordholm, and S. Mishra. Entropy stable scheme on two-dimensional unstructured grids for Euler equations. *Commun. Comput. Phys.*, 19(5):1111–1140, 2016.
- [33] F. Rieber. A low-Mach number fix for Roe’s approximate Riemann solver. *J. Comput. Phys.*, 230(13):5263–5287, 2011.
- [34] S. Samantaray. Asymptotic preserving linearly implicit additive IMEX-RK finite volume schemes for low Mach number isentropic Euler equations. arXiv:2409.05854, 2024.
- [35] S. Schochet. Fast singular limits of hyperbolic PDEs. *J. Differ. Equations*, 114(2):476–512, 1994.
- [36] E. Tadmor. The numerical viscosity of entropy stable schemes for systems of conservation laws. I. *Math. Comput.*, 49(179):91–103, 1987.
- [37] E. Tadmor. Entropy stability theory for difference approximations of nonlinear conservation laws and related time-dependent problems. *Acta Numer.*, 12:451–512, 2003.
- [38] E. Tadmor. Entropy stable schemes. In R. Abgrall and C.-W. Shu, editors, *Handbook of Numerical Methods for Hyperbolic Problems*, volume 17 of *Chapter 18 in Handbook of Numerical Analysis*, pages 467–493. Elsevier, 2016.
- [39] M. Tang. Second order all speed method for the isentropic Euler equations. *Kinet. Relat. Mod.*, 5(1):155–184, 2012.

- [40] N. Wintermeyer, A. R. Winters, G. J. Gassner, and D. A. Kopriva. An entropy stable nodal discontinuous Galerkin method for the two dimensional shallow water equations on unstructured curvilinear meshes with discontinuous bathymetry. *J. Comput. Phys.*, 340:200–242, 2017.
- [41] G. Yan, S. Kaur, J. W. Banks, and J. E. Hicken. Entropy-stable discontinuous Galerkin difference methods for hyperbolic conservation laws. *J. Comput. Appl. Math.*, 422:114885, 2023.
- [42] H. Zakerzadeh and S. Noelle. A note on the stability of implicit-explicit flux-splittings for stiff systems of hyperbolic conservation laws. *Commun. Math. Sci.*, 16(1):1–15, 2018.
- [43] J. Zeifang, J. Schütz, K. Kaiser, A. Beck, M. Lukáčová-Medvid’ová, and S. Noelle. A novel full-Euler low Mach number IMEX splitting. *Commun. Comput. Phys.*, 27(1):292–320, 2019.